1-1-2013

Fabrication Of Two-Dimensional Nanostructures On Glass Using Nanosphere Lithography

Elmer Jim Wang
Wayne State University,

FABRICATION OF TWO-DIMENSIONAL NANOSTRUCTURES ON GLASS USING NANOSPHERE LITHOGRAPHY

by

ELMER WANG

THESIS

Submitted to the Graduate School

of Wayne State University,

Detroit, Michigan

in partial fulfillment of the requirements

for the degree of

MASTER OF SCIENCE

2013

MAJOR: ELECTRICAL ENGINEERING

Approved by:

_____

Advisor Date

ACKNOWLEDGEMENTS

I want to thank my friends and family that encouraged and supported my journey to obtain a Master's of Science. I want to note the help I received from Elson Liu for helping me and giving me advice when I needed it throughout the course of obtaining my Master's degree. I want to also thank Christopher Thrush for all the help he provided with the AFM and spectrometer measurements. He was an integral part of my successful completion of my master's thesis. And I especially want to thank Professor Yang Zhao for giving me a chance to prove myself and acquire this degree. He believed in me and the fruits of my labors into an unexplored frontier of etching glass with a nanoparticle mask are represented in this thesis document.

TABLE OF CONTENTS

LIST OF TABLES

LIST OF FIGURES

CHAPTER 1

INTRODUCTION

Currently the fields of nanotechnology and nanomachining are advancing at a rapid pace. With an emphasis on looking for novel materials with the desired properties as well as making things more portable and public demand for more features to be packed into their devices, fabrication of nanoscale structures is becoming an important field of research. [1]

A two-dimensional (2D) nanostructure is a structured surface which has very different properties when compared to their bulk counterparts. 2D nanostructures typically have feature sizes smaller than 200 nm. The scale and structure of these artificial materials allow for some unique and useful applications of the technology. One example is the creation of a material with a very low and specified optical refractive index. Another related application would be the enhanced transmittance of glass and antireflection coatings for displays on various types of functional surfaces. There are also applications in bio-mimicry and artificial nanomaterials. Because of the many useful and interesting properties and applications, the study of 2D nanostructures is a very important research project.

Existing technologies for the fabrication of 2D nanostructures requires exorbitant amounts of time and/or are extremely expensive to create large areas of patterned features. One prominent technology, for example, is electron beam lithography, which, although is versatile for creating various nanoscale patterns over a small area, is forbiddingly expensive and slow for making large-area nanostructures. On the other hand, glass materials that are optically transparent are difficult to machine, and there are a limited number of ways to modify them. This project is to study a feasible process and develop low-cost techniques for fabricating 2D nanostructures on optical glass using nanosphere lithography.

1.1 Purpose

The primary impetus behind this research is to create fast and inexpensive technology that can be used on most glass materials (such as crown and soda-lime glass). This will allow surface modifications in bulk quantities that would be required for various applications and mass production. The creation of nanostructures over large areas within a short amount of time would make this a viable and preferable process compared to existing technologies.

1.2 Review of Methods for Creating 2D Nanostructures

Various methods of creating microstructures have emerged in the past century. Most of these methods have limited success in creating 2D nanostructures. A brief review is given here.

1.2.1 Photolithography

Photolithography is a common technology that can be found in cleanrooms around the world. Using an optical beam, light is used to create masks in polymer that are later used to etch into micro-structures on substrate.

The resolution of the features within a structure created using photolithography is determined by the following equation:

$$CD = k_1 * \frac{\lambda}{NA}$$

Where CD is the minimum feature size, k_1 is a process-related coefficient, λ is wavelength of the light used, and NA is the numerical aperture. By decreasing the wavelength and increasing the numerical aperture, the minimum features on a substrate can be decreased. Typical feature size limit of optical lithography using visible light is 250-300 nm. This is given by the ideal equation for resolution of feature sizes:

$$R = 0.61\frac{\lambda}{NA}$$

Where R is the radius of the feature size (nm) and the 0.61 is obtained from the Rayleigh-Abbe limit. However, due to system imperfections this limit is likely to be larger.

To make structures with feature sizes less than 250 nm, visible light is no longer a viable source of illumination. The solution was to use deep ultraviolet light and increasingly shorter wavelengths of laser. [2] [3] [4] The equipment to make smaller than 250 nm feature sizes becomes expensive to purchase and install. In addition, new material for masks and projection system would be required.

For feature sizes below 50nm, substrates can no longer be processed in air, and require liquid immersion techniques to be combined with excimer lasers. This creates more complex steps, training, and more cost as companies continue to use optical lithography to pattern nanoscale features.

1.2.2 Electron Beam Lithography

Electron beam lithography is a very accurate and precise method for creating nanostructures with a resolution of a few nanometers. Many samples of 2D nanoscale structures have been fabricated using this technology, but the area of these features is usually very small. This is because the technology a very time-intensive scanning process. [5] [6] [7] While the structures that are created can be extremely accurate, using electron beam lithography, the time required for its creation is enormous. The entire pattern for the structure is not written at once by projection, as in photolithography. Instead the electron beam moves one location at time in a line and scans the pattern into the substrate. The time for exposure is given by the following formula:

$$D * A = T * I \text{ [8]}$$

Where D is the dose, A is the area exposed, T is the time to expose the substrate, and I is the beam current. This equation only considers the exposure time and none of the other mechanical requirements that may be a factor during writing of a pattern. In order to create a nanostructure that is 1 cm^2 using an electron dose of 10^{-3} Coulombs/cm^2 and beam current of 10^9 Amperes it would take 12 days. This is not practical for large areas of nanostructures. [9]

1.2.3 Nanosphere Lithography

Nanospheres have only recently been introduced into the scientific community. It is a new technology compared to the above mentioned methods. For lithography, the nanospheres of uniform size are assembled into a monolayer of spheres to be used as a mask. To create the mask, the first step is to have the nanospheres self-assemble themselves into a uniform monolayer. This allows for the fabrication of arrays with very precisely controlled spacings based on the nanosphere diameters and packing efficiency. The holes between the particles create the mask for etchants or other patterning technologies to reach the substrate. After the mask is made, depending on the substrate, different methods can be used to etch away the substrate to create a uniform, honeycomb spike structure. Based on the size of the nanospheres, the structure of the resulting mask can change dramatically for various applications. There are several methods for the creation of nanoparticles, and their size can be tailored to the customer that orders them.

The resolution of nanosphere lithography (NSL) is limited by the size of the nanosphere particles used for the mask. The smallest size of polymer nanospheres is approximately 20 nm, whereas uniform gold particles can be as small as a few nanometers. Through the mechanism of self-assembly, nanosphere masks can be created over a large area from a few minutes to a few hours.

After reviewing these other technologies, it appears that using nanosphere lithography is the best choice for creating 2D nanostructures with desired feature size and area. [10] [11] [12] [13]

1.2.4 Nanoimprinting

Another method for patterning 2D nanoscale structures is nanoimprint lithography. This is a mechanical process for creating nanoscale patterns through deformation of resist and associated processing steps. While the process is low cost with high throughput and resolution, the stamp needed to create the pattern is very expensive, especially for large stamps, and usually involves one of the processes mentioned in the above sections.

Another problem with nanoimprinting is the quality of the lithography pattern. Material transport from substrate to mask is very different for positive and negative stamps. When the pattern is small and periodic this method is very effective, however as soon as there are large differences in the pattern, material transport of the process limits the quality of the final pattern. [14] [15] [16] [17] [18] [19]

1.3 Two-Dimensional Nanostructures on Glass

There are many reasons to study and create 2D nanostructures on glass. First, glass is a very commonly used optical material for substrates or windows. This is because it is cost-effective, transparent to visible light, and chemically stable. There are many applications using nanostructures to modify the surface material properties of a glass substrate.

One of the main motivations for creating 2D nanostructures on glass is the ability to create tunable refractive indices in the surface of a glass substrate. This would allow related applications such as the enhanced transmittance of glass and antireflection coatings and cladding

material for optical waveguides. Using these methods, it is also possible to create artificial nanomaterial as well as applications involving bio-mimicry.

1.3.1 Common Optical Glass

Glass is chemically a very stable material. While most glass is amorphous, the crystalline structures formed by the silicon di-oxide allows for very stable and durable materials. With commercial glass, there are usually impurities introduced into the glass to reduce cost. Soda-lime glass and crown glass are two very common types of glass available commercially. Soda-Lime glass is typically constituted of 73% SiO_2, 14% Na_2O, 9% CaO, 4% MgO, 0.15% Al_2O_3, 0.03% K_2O, 0.02% TiO_2, and 0.1% Fe_2O_3. All these impurities will affect how easily the glass is manipulated with chemicals.

Soda-Lime glass is a very common material that is used in a multitude of applications. It is a common material for windows, sensors, solar cells, display devices, and anything requiring optical translucency. Being able to modify glass surface via nanosphere lithography, it can lead to many other applications of a popular and inexpensive optical material.

1.3.2 Fabrication of Two-Dimensional Nanostructures on Glass

1.3.2.1 Nanosphere Lithography

Using nanosphere masking, a uniform monolayer of particles resembling a honeycomb was created. The size of the particles determined the parameters of the mask. The packing efficiency and size of the particles allowed for small gaps in the layer that would become the mask pattern for etching the substrate.

This procedure for creating a self-assembled nanosphere mask has been performed before. [20] [21] [22] [23] [24] [25] [26] [27] [28] This process relies heavily on attractive capillary force because of the size of the spheres that are being used.

Because glass is a very stable and hard to affect material, there are very few chemical compounds that are able to etch glass and otherwise modify its structure. Fortunately, Hydrofluoric Acid has been used for decades to modify glass substrate. Though this has been used for glass in bulk, there has been little research done on creating structures with nanoscale features. This will be the first systematic research effort to study the etching of 2D structures on glass using nanosphere lithography. [29] [30] [31] [32] [33] [34]

1.3.2.2 Hydrofluoric Acid Etching

Hydrofluoric acid (HF) is the most common chemical used to etch glass. The etching process is characterized by the following two equations:

$$SiO_2 + 4\ HF \rightarrow SiF_4\ (g) + 2\ H_2O$$

$$SiO_2 + 6\ HF \rightarrow H_2SiF_6 + 2\ H_2O$$

As the glass interacts with HF, the HF will release water and SiF_4 in a gaseous form and remove parts of the glass that is in contact with the HF. Usually glass is masked and submerged into liquid HF so that the HF is only in contact with the surfaces that require etching. As the HF interacts with the glass, any water byproduct is just mixed into the HF solution which keeps the water from blocking the glass surface from being etched further. This becomes a concern when we apply the vapor phase of hydrofluoric acid.

1.3.2.3 Vapor Phase Hydrofluoric Acid

Using liquid hydrofluoric acid is a very common practice when it comes to oxides; however HF vapor etching is far less common, has a slower etch rate, and is more difficult to control. [35] However, the vapor form of hydrofluoric acid is an effective tool in NSL for etching glass over large areas. The gas interacts with the glass in a way that doesn't cause the nanoparticles to be moved or otherwise disordered. If we used the liquid phase of hydrofluoric acid, the nanoparticles would be washed off and there would be no mask preserved to etch a nanostructure into. The vapor pressure of hydrofluoric acid [30.7 mbar (23 mmHg) at 20°C (68°F)] allows it to convert to vapor form from liquid at room temperature. This makes it ideal for etching glass without any special equipment.

While not much research has been done with vapor phase etching in nanostructure fabrication, the research herein demonstrates that it is a feasible solution. This technology appears to be the most effective and inexpensive way to etch glass without damaging the nanosphere mask.

1.4 Applications

1.4.1 Anti-Reflection Coating

Many electronics and other devices require the use of optics. One major problem that has plagued the design of optical components is the unwanted reflection off the surface of the optical elements. The primary solution has been to coat the surface with a layer of intermediate thin film to enhance the transmission of the light through the optical element. The index of refraction that is chosen is governed by the equation:

$$n_f = \sqrt{n_o n_s} \quad \text{(Eq. 1.1)}$$

where n_f is the index of refraction of the thin film, n_o is the index of refraction of the incident medium, and n_s is the incident of the substrate the film is applied to. This equation determines how to completely cancel out the reflected light wave through the use of $\frac{\lambda}{4}$ thickness coatings. [36] In the case of ordinary glass, it has an index of refraction $n \approx 1.5$ and air has an index $n = 1$. Following Eq. 1.1, we can see that the ideal film index would be $n \approx 1.23$. Unfortunately there is no material in nature that has this value. The closest and most practical substance is MgF_2, and it has an index of $n = 1.38$. Techniques have been developed in order to further reduce reflection, such as using multi-layer anti-reflection coatings where additional coatings of $\frac{\lambda}{2}$ thickness material have a high index, followed by a low-index to further improve transmission.

By using nanoparticles to mask the surface of a substrate (in this case ordinary glass) and etching the material a surface modification is created that causes the surface of the substrate to behave as an anti-reflection coating. The benefit of using this type of technology to the coatings is the ability to tune the index of refraction of the etched nanostructured layer that has been created. [37] [38] [39] [40] [41] [42] In preliminary tests using silicon, it has been shown that the layer being etched can reach an index of refraction of about n=1.27. This reflective index can also be tuned further by manipulating the nanosphere mask and etching amount. The effective refractive index at normal incidence of the surface modification can be calculated by using a simplified approach derived from the equation of a one-dimensional subwavelength grating structure –

$$n_2^* = [n_1^2(1 - F) + n_2^2 F]^{\frac{1}{2}}$$

Where n_1 is the refractive index of air, n_2 is the refractive index of polystyrene, and F is the fill factor of polystyrene nanoparticles, which is the volume percentage of nanoparticles in the film. [43] This demonstrates that an artificial reflective index can be created to completely cancel out

a reflected wave. This idea has already been used in diffractive optics and on semiconductor substrates. [44] [45] [46] [47] By applying this same principle to glass, we hope to create a similarly tunable layer of modified material. [48] [49] [50] [51] [52] [53] [54] [55]

1.4.2 Bio-mimicry

Bio-mimicry is the process by which researchers create structures or products that mimic those that exist naturally in animals and plants. Using principles from bio-mimicry we are able to reproduce the benefits of this nanostructure for non-organic products. The moth eye and the lotus leaf are two examples of what the results of this research on surface modification imitate. A moth's eye is typically a 300nm hexagonal nanostructure of photoreceptors. This unique structure gives it anti-reflection properties in order to obscure itself from predators. The eye is typically a compound eye and has larger viewing angles.

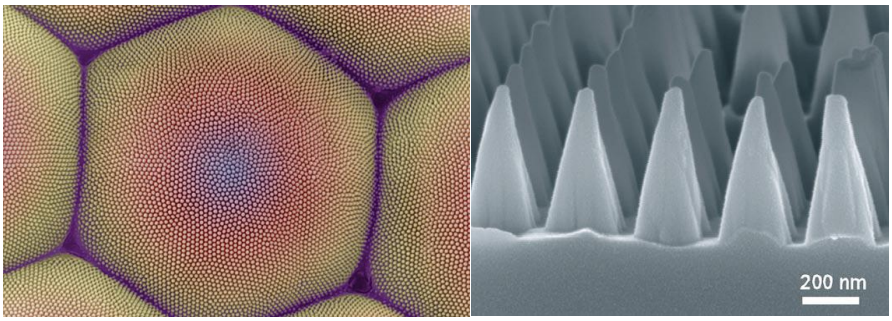

Figure 1: (left) Moth Eye, (right) SEM of Moth Eye

The lotus leaf exhibits a non-periodic nanostructure on its leaves that create a hydrophobic effect for self-cleaning. [56]

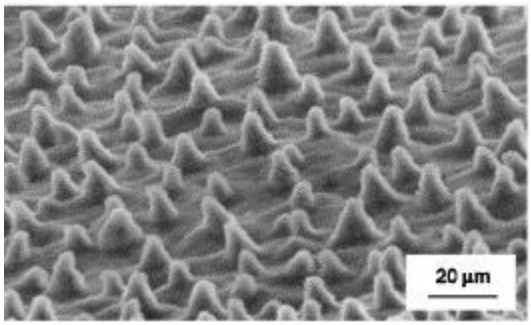

Figure 2: SEM of Lotus Leaf

These formations in nature are essentially the negative imprint of the mask that was created in this research project.

1.4.3 Waveguides & Cladding Material

In optical waveguide applications, cladding for the waveguide has to be a low refractive index. This is usually done via another coating or by drawing two separate materials together. This process can be simplified by surface modification of the waveguide itself. This is accomplished by creating a low refractive index layer on the waveguide material using the results of this research.

CHAPTER 2

Methods and Techniques

2.1 General Procedure

The first objective of this research was to create a uniform mono-layer of, approximately 200 nm, polystyrene nanoparticles on glass substrate. This would provide the mask that would be used for etching the surface modification. Various methods of creating a nanoparticle coat were researched in order to find the most effective way to coat a substrate with a nanoparticle mask. Slide-coating was the first approach studied, followed by drop-slide coating, and then wedge-coating. It was determined that slide-coating was most consistent. This method was selected because of its simplicity and quality for creating a monolayer coat with 200 nm nanoparticles.

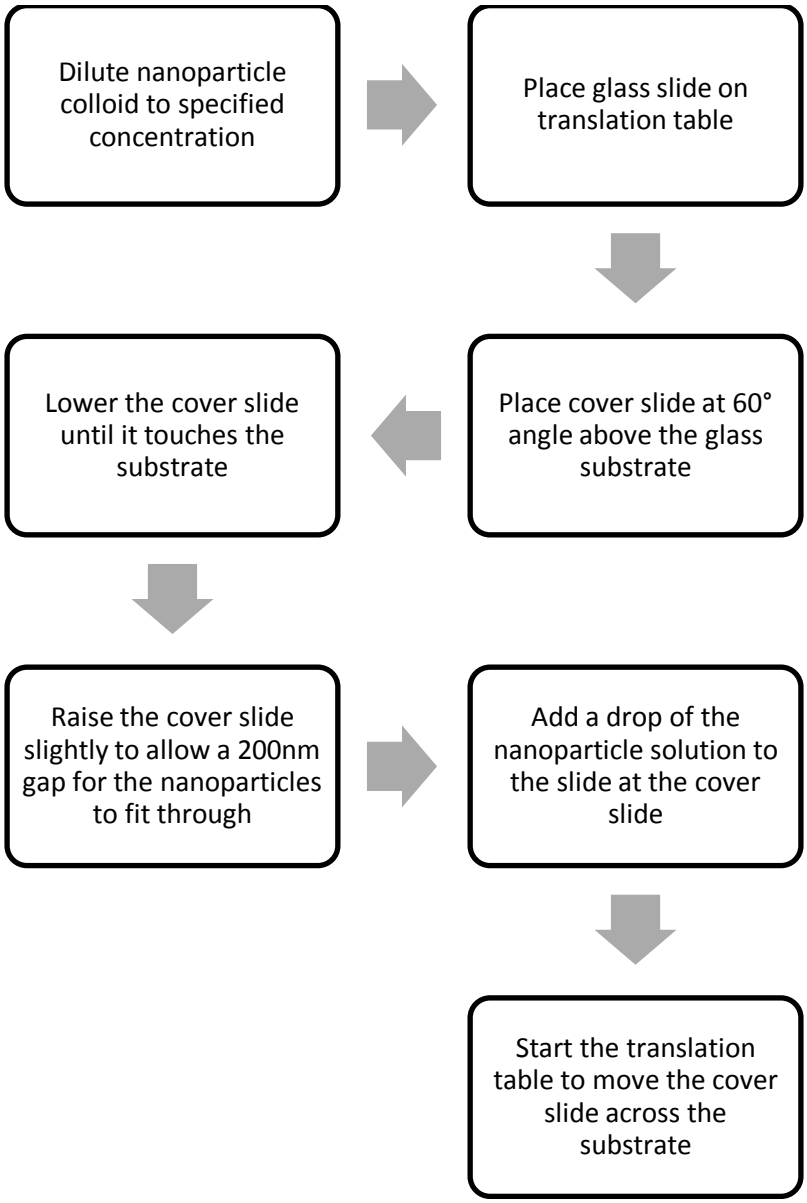

Figure 3: Flow chart of slide coating procedure

Figure 3 is showing the flow chart of the slide coating procedure used in this research. Section 2.2 describes each of these steps in detail. After a successful coat, the sample was placed above a petri dish of hydrofluoric acid (HF). HF is one of the few chemicals that can etch SiO_2. Instead of applying the HF directly to the glass, as is typical, it was applied via the vapor phase. This method allows for the use of HF without washing off the particle coat. It also creates a more controllable etch rate than that of liquid HF etching.

2.2 Nanoparticle Mask

There are multiple methods available to create 2D monolayer nanoparticle coats on substrates. One of the popular methods is spin coating. This approach was considered, but the process of spin-coating would be an inefficient use of the nanoparticle solution. Spin coating would reliably produce a consistent coat, but a majority of the nanoparticle solution would become waste as it is spun out to the sides and unable to be reclaimed.

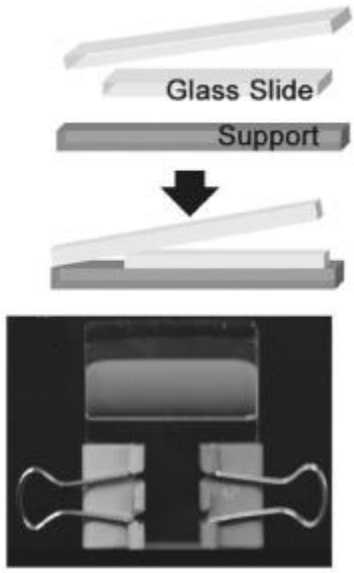

Figure 4: Diagram of the Wedge Method [57]

Another method that was implemented involved creating different profiles for the solution between a ceiling slide and the substrate – the Wedge method (Fig. 4). The gap between these two slides and how it's implemented would create different evaporation profiles. The profile of the solution and its evaporation speed would determine how well ordered the particles would become coated. This method was tried for 50 slides with various angles and offsets for the top slide in order to create slightly different meniscus profiles. This method was much slower than the others, but since no special equipment was used, it was possible to run multiple trials

simultaneously. This method was dropped in favor of slide-coating because of the difficulty of controlling evaporation rates without specialized humidity and temperature equipment.

Slide-coating was chosen as the method for creating 2D nanoparticle masks and the process of slide-coating is as follows. The substrate was placed on a motorized translation stage (MC1000e-1), and a cover slip angled at 45° from the substrate was used to spread nanoparticles into a monolayer mask.

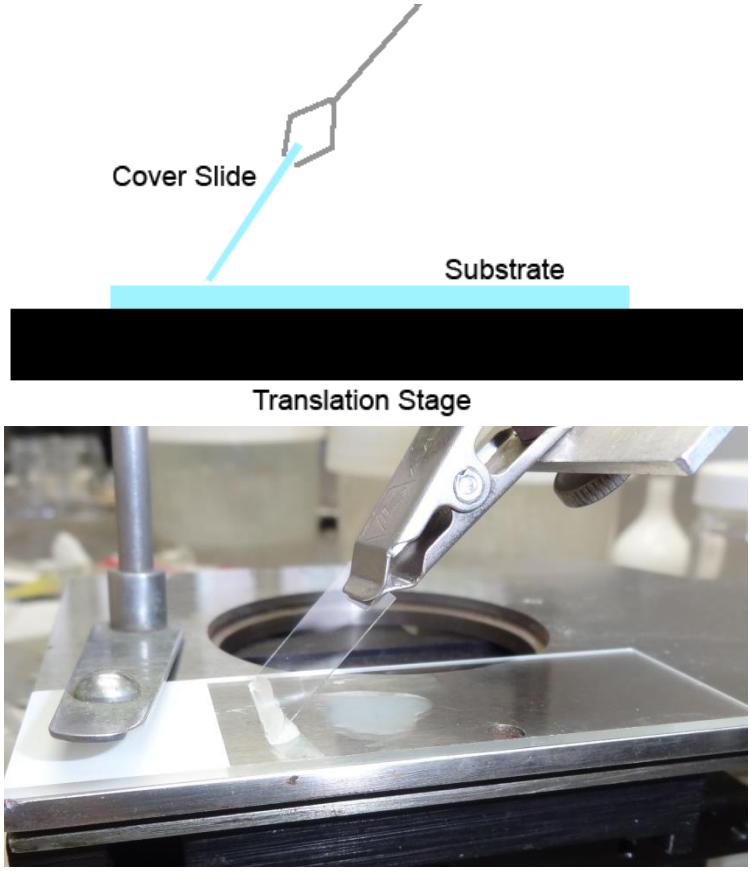

Figure 5: Slide-coating. Top: Diagram of Setup. Bottom: Picture of actual set-up.

The cover slip is positioned with a gap slightly more than a 200 nm between it and the substrate, this allows nanoparticles to pass through the gap with only one layer. A drop of the solution would then be placed behind the cover slide, and the translation stage would move so that the cover slide would be spreading the solution of nanoparticles across the slide. The

capillary action would keep the water behind the cover slide while the nanoparticles would escape and align themselves via the gap created by the cover slide and the substrate.

Table 1: Settings for slide coat

Slide #	Method for Coating	Speed Setting	Actual Speed	Dilution Concentration
96	Slide Coating	Slow	26 µm/s	1/100
97	Slide Coating	Slow	26 µm/s	1/100
98	Slide Coating	Slow	26 µm/s	1/100
99	Slide Coating	Slow	26 µm/s	1/100
100	Slide Coating	Slow	26 µm/s	1/100

Table 1 presents the conditions for which monolayer coatings for slides was created. Polymer nanospheres were purchased from Bangs Laboratories with a 10% solid in colloid concentration and mean diameter of 200nm. Here the speed of the slide movement is 26 µm/s, and the diluted concentration is 1% of original colloid concentration (10%). Most of the slides ended up with good quality coating, but there were a few that contained less than one layer of coating, or had overlapping layers. This method was the most consistent to reproduce a successful coat. It took approximately 5-45 minutes per slide, and could be run with minimal to no supervision. The best quality coatings were produced at 45 minutes per slide.

After the slides were coated, the atomic force microscope was used in order to examine the structure that resulted from each coating run. Below in Fig. 6 is a 2x2 µm AFM picture that was taken.

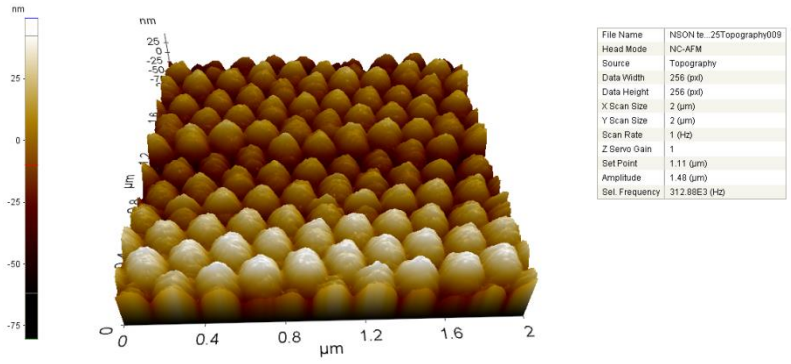

Figure 6: 3D render of a uniform nanostructure.

In Figure 6, the nanoparticles form a nice ordered structure after the slide coat. This is the basis for our mask. In Figure 7, a line profile is taken to demonstrate that the spacing is logical. With each nanoparticle being ~205 nm, we expect approximately 5 particles per 1 µm; the line profile demonstrates that. There is a slight variation in height, but this is likely due to uneven manufacturing on the nanoparticles themselves, a calibration error with the AFM, or the slide/slide platform is not 100% level, and so the AFM would pick up the minute change in height for the profile.

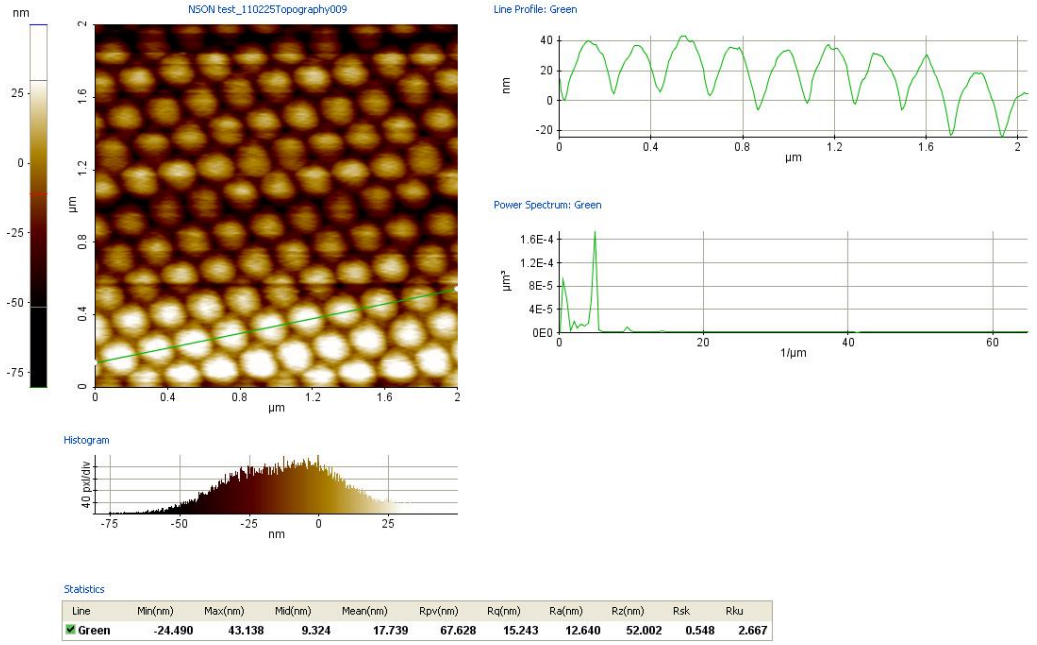

Figure 7: Line profile of Figure 6

Figure 8 conveys the structure of the nanoparticle mask on a larger scale. This particular scan was done near the edge of the deposit to make sure the edges of a particular mask section was not piling up and thus becoming more than 1 layer. Figure 9 shows a 3D representation of a more centrally located mask section. It should be noticed that there is a variation in striations that seem to make some horizontal sections of the area look as though they have a different height. But, as stated above, this can be accounted for by uneven slide placement on the equally uneven slide platform.

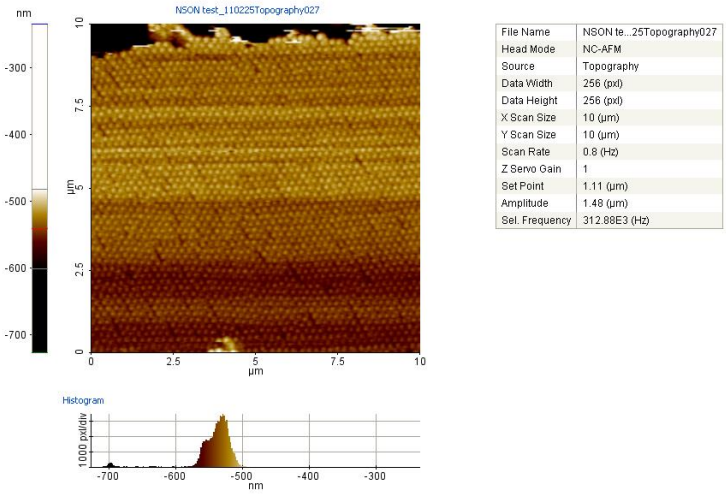

Figure 8: 10x10 µm scan of a uniform nanoparticle structure

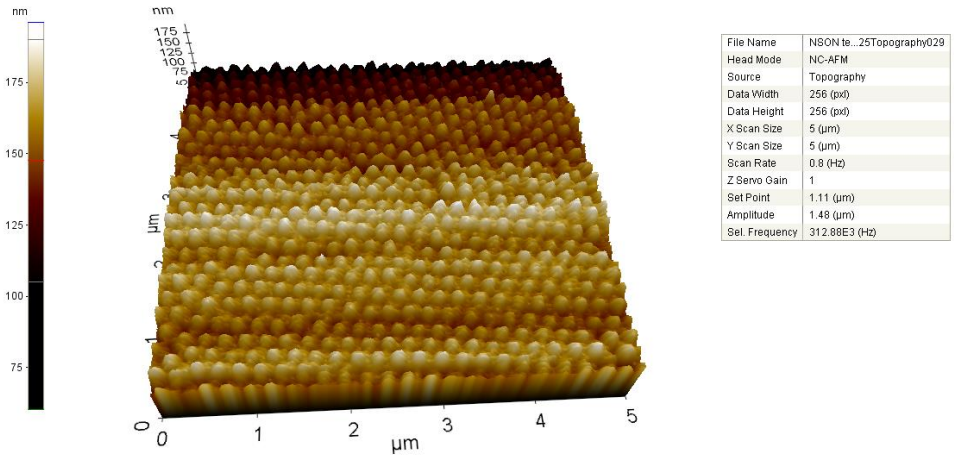

Figure 9: 5x5 µm of a nanoparticle mask

All these examples have been for slides that were covered almost fully. The other acceptable outcome of a slide coat was a slide that was covered by less than 1 layer. Figures 10, 11, and 12 illustrate how some of these slides appeared under the AFM examination.

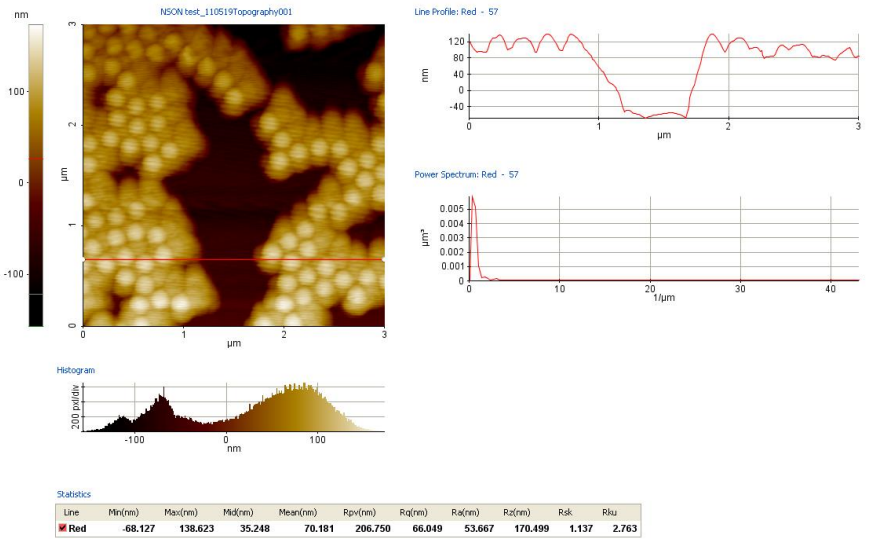

Figure 10: Profile of a 3x3 µm AFM scan

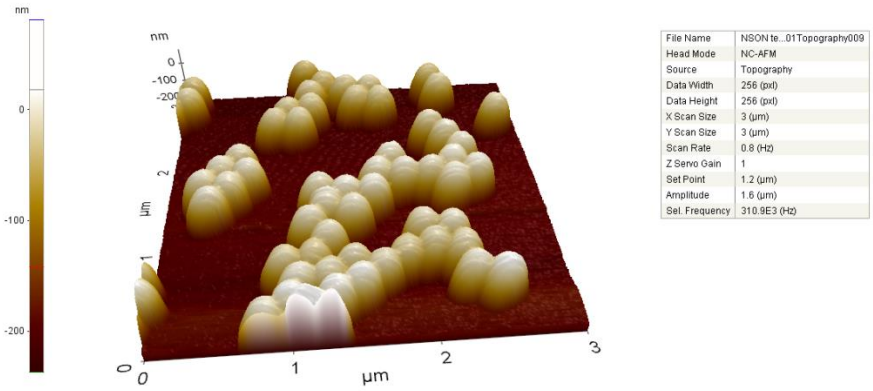

Figure 11: 3D view of another <1 layer of nanoparticles

By observing Figures 10 & 11, it is clear that the slide is not as fully coated as they were in Figures 6, 7, 8, and 9. The nanoparticle coating process while consistent does not always produce a perfect coat. Having less than 1 layer of particles may still work, as there are areas of the slide that are still masked that can still be experimented on. Through examination of the line profiles in Figure 10 and 12 it is shown that they are correctly spaced for a uniform nanoparticle mask, where the particles are actually conglomerated. This is much clearer in Fig. 10, whereas Fig. 12

exhibits some effects of ghosting. This ghosting of the image is likely due to mechanical vibrations during the scanning process. Even the slightest vibration can be picked up by the AFM. But by examining the major peaks of the scan, it is plain to see that the nanoparticles are spaced the correct distance.

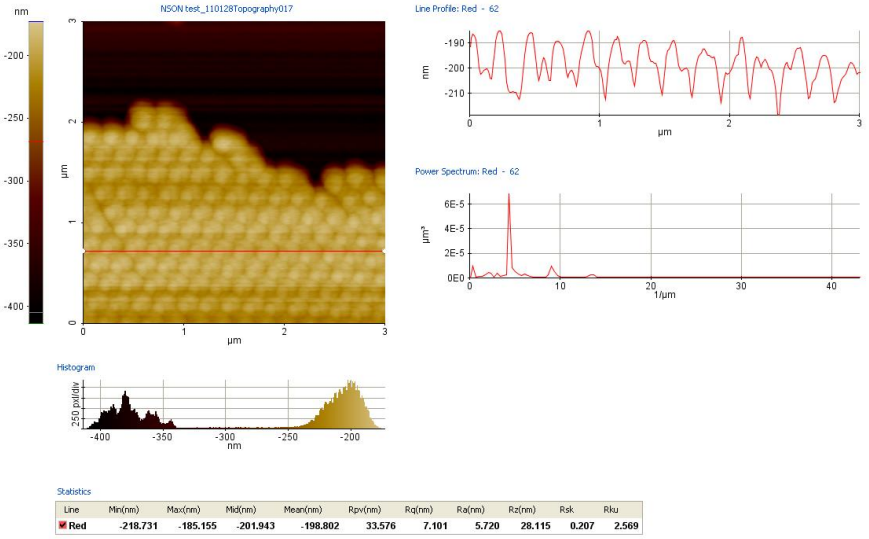

Figure 12: Edge of a deposit of nanoparticles; 3x3µm scan

In many of these AFM pictures, the valleys of the profiles never go all the way to zero. This is because of the mechanical limitations of the tip of the AFM.

2.3 Hydrofluoric Acid Vapor Etching

Hydrofluoric acid is the most common chemical used to etch glass. For this application, we want to use the vapor form of hydrofluoric acid since using the liquid form would wash off the nanoparticle mask that was created in the last step. The vapor phase is just as effective as the liquid form when etching glass. The etching process is characterized by the following two equations:

$$SiO_2 + 4\ HF \rightarrow SiF_4\ (g) + 2\ H_2O$$

$$SiO_2 + 6\ HF \rightarrow H_2SiF_6 + 2\ H_2O$$

When HF is placed in a reservoir it passively generates into its vapor phase. 20 mL of HF was poured into a petri dish and left for 5 min to let the vapors begin to form. If etching is started immediately after pouring the HF, the sample will become over-etched because the vapors that are generated are too concentrated.

The setup for the etching process involves a computer controlled arm that will alternate the position of the sample. Figure 8 shows how all the components were positioned for the etching process. On the two ends of the arc of the arm are a hot plate and the petri dish with HF in it. The hot plate is to evaporate the H_2O byproduct of the glass etching. If excess H_2O accumulates on the sample, a thin film of H_2O will prevent the HF vapors from reaching their intended target. The substrate is placed 11.5 cm above the hot plate that has been set to 200° C. Since the substrate is in a fume hood and is a considerable distance away from the hot plate, the temperature is elevated to account for the heat lost. The petri dish at the other end of the path is placed so that the substrate is approximately 1.2 cm from the surface of the acid.

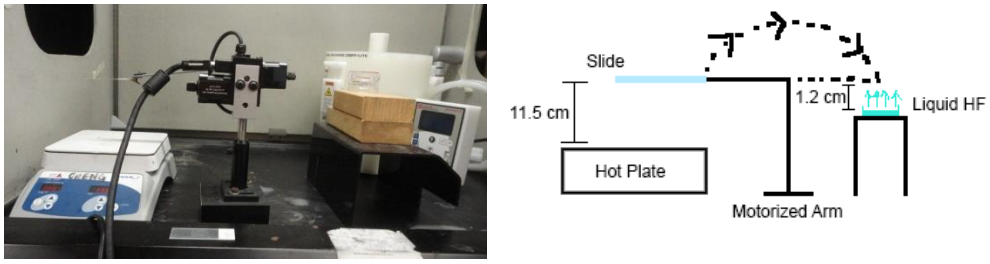

Figure 13: Setup for etching glass slides

The procedure for etching involved setting the time spent above the acid, the time spent above the hot plate, and then the number of cycles of hot plate and acid interaction there would be. The amount of time spent above the acid varied while maintaining a constant hot plate exposure of 30 seconds per cycle. HF acid is very potent, and even in vapor form the substrate only had to be exposed for ten seconds or less before the risk of over-etching became a concern. When the

etching cycles were completed, the substrate would rest over the hot plate and then removed to be examined under the AFM with the nanoparticle mask still on. Then the mask would be washed off and examined by AFM again. Examining the substrate with the mask still on the substrate under the AFM would allow inspection to see if the H_2O that formed from the etching process had manipulated the structure of the nanoparticle mask.

Figures 14-21 are examples of what the slide looks like after it has been etched. The nanoparticles have remained on the slide in order to ensure that their structure has remained intact during the etching process. Since H_2O is a product of HF etching of glass, the nanoparticles have the possibility of shifting and thus changing the uniform structure and, consequently, the mask mid-etch. Figure 14 and 15 are from the same slide. The line profile demonstrates that there is some degradation on the nanoparticle, but not enough to deform the overall mask. Also there are 5 humps for approximately every 1 µm. The profile's slight deviation is due to human error while drawing the measuring line, since the line isn't going through the center of every single particle. It can be seen from both figures, the surrounding glass around the nanoparticles has been etched and been chemically machined. This similar roughness can be seen in figures 16 and 17. Even on a 10x10 µm square the roughness of the glass can be seen and also the linearity of the nanoparticles. Figure 17's line profile shows that the particles are still all approximately the same height barring a vertical gradient that is likely caused by an unsmooth platform. The line profile would reflect the correct spacing if the nanoparticles were all together, but this is <1 layer of mask and thus some non-uniformity is to be expected between or near the spaces where there is a void of particles.

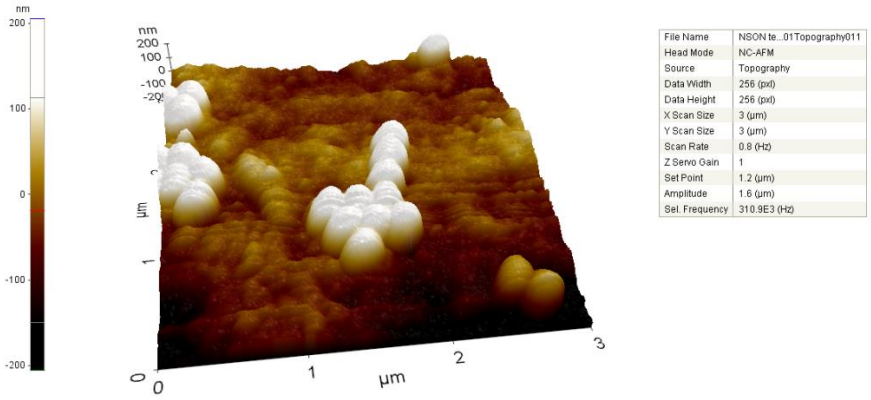

Figure 14: 3D representation of 3x3 µm area

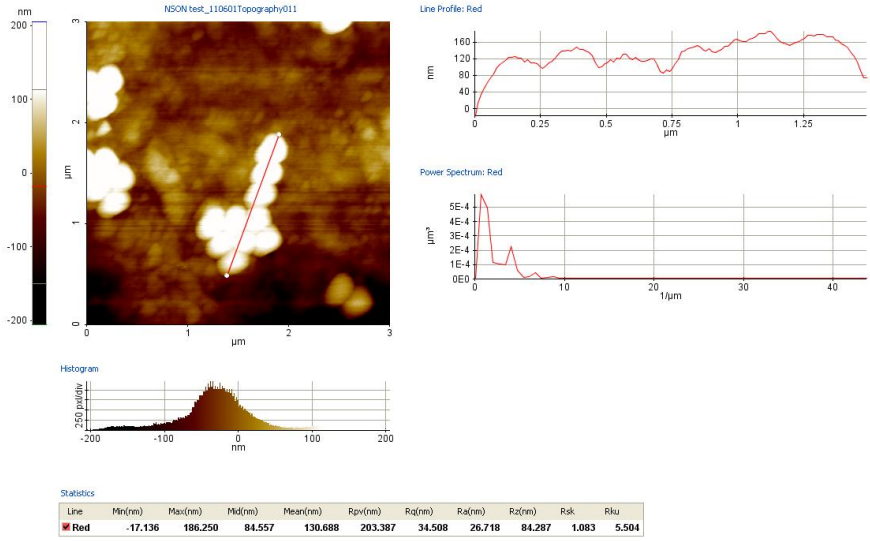

Figure 15: Line profile of 3x3 µm area scan

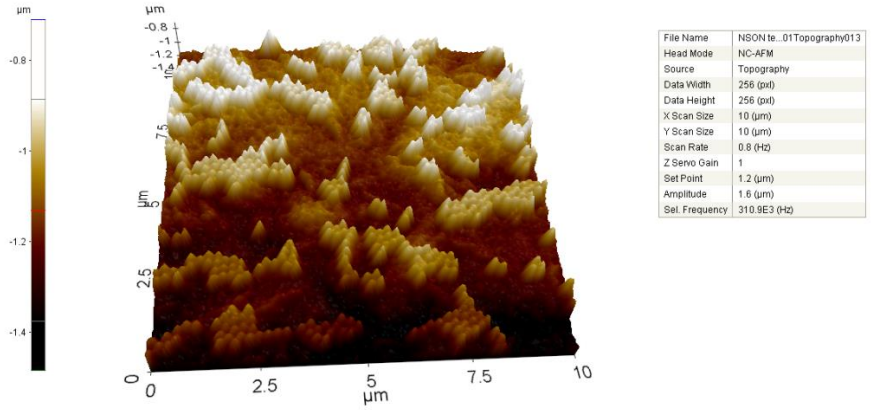

Figure 16: 3D representation of 10x10 µm scan

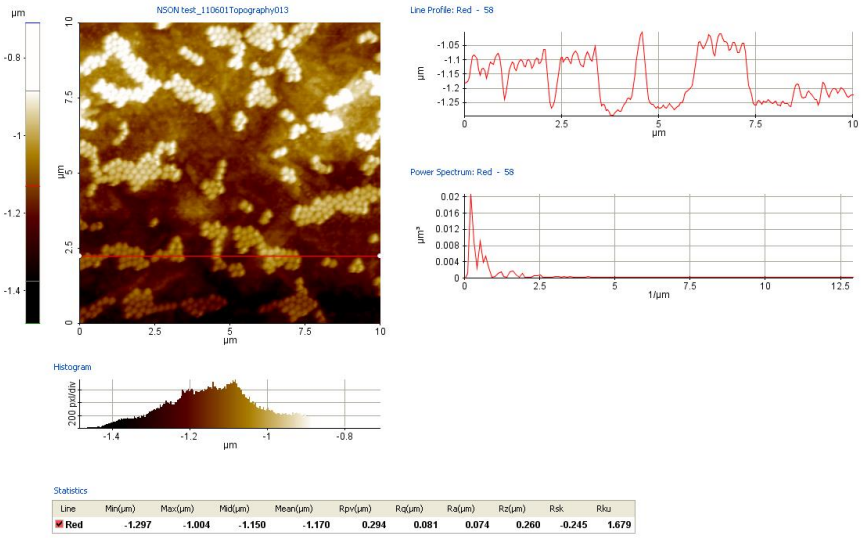

Line	Min(µm)	Max(µm)	Mid(µm)	Mean(µm)	Rpv(µm)	Rq(µm)	Ra(µm)	Rz(µm)	Rsk	Rku
Red	-1.297	-1.004	-1.150	-1.170	0.294	0.081	0.074	0.260	-0.245	1.679

Figure 17: 10x10 µm line profile

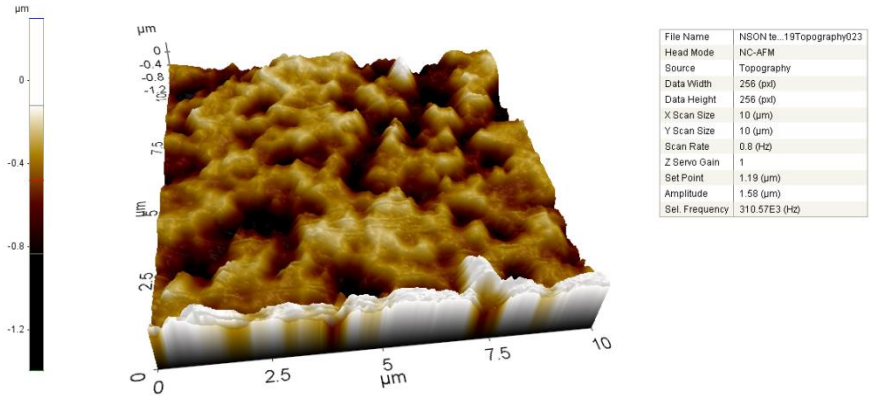

File Name	NSON te...19TopographyO23
Head Mode	NC-AFM
Source	Topography
Data Width	256 (pxl)
Data Height	256 (pxl)
X Scan Size	10 (µm)
Y Scan Size	10 (µm)
Scan Rate	0.8 (Hz)
Z Servo Gain	1
Set Point	1.19 (µm)
Amplitude	1.58 (µm)
Sel. Frequency	310.57E3 (Hz)

Figure 18: 10x10 µm 3D topography

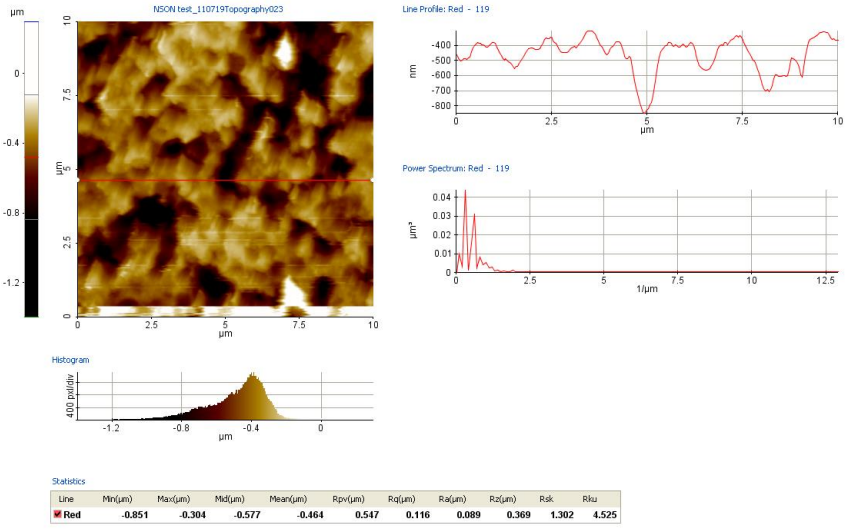

Figure 19: 10x10 µm line profile

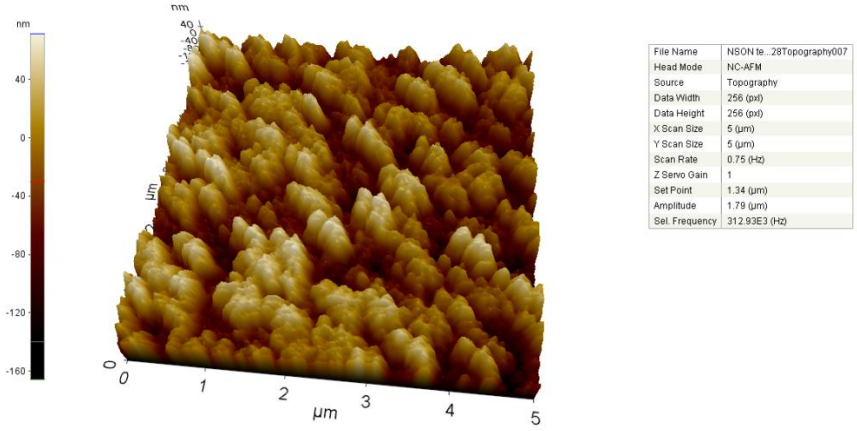

Figure 20: 5x5 µm 3D representation of Etched slide

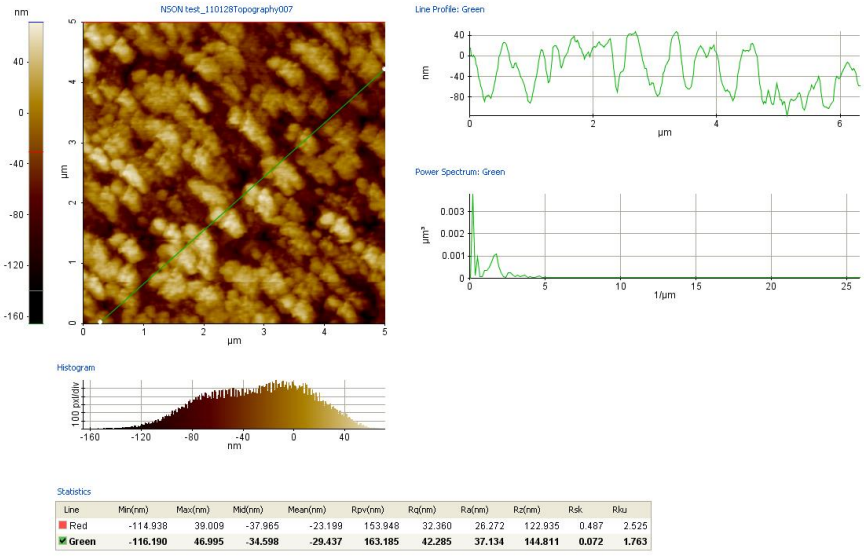

Figure 21: Line profile of 5x5 µm etched sample

2.3.1 Etching Rates of Vapor HF for Nanostructures

It is interesting to study the etching rate of vapor phase HF for nanostructure and compare it to that of liquid HF and for bulk material.

Table 2 demonstrates the time over the vapors versus the depth from etching. The data for this was gathered via the horizontal line profile between the highest point and the lowest point on particular slides and averaged. The reason for taking multiple data points on a horizontal line profile accounts for the vertical imbalance that has been observed on the AFM.

Table 2: Etching data

Slide #	Distance from Acid (cm)	Distance from Heater (cm)	Time over Acid (s)	Time Over Heat (s)	# of Cycles	Total Time over Acid (min)	Average Etching Depth
89	1.2	11.5	5	30	12	1	70
92	1.2	11.5	5	30	24	2	123.3333
87	1.2	11.5	5	30	60	5	186.6667
88	1.2	11.5	5	30	120	10	266.6667
91	1.2	11.5	5	30	180	15	282.5
90	1.2	11.5	5	30	240	20	591.6667
93	1.2	11.5	5	30	36	3	N/A
96	1.2	11.5	5	30	12	1	65
97	1.2	11.5	5	30	15	1.25	60
98	1.2	11.5	5	30	18	1.5	82.5
99	1.2	11.5	5	30	21	1.75	121.25
100	1.2	11.5	5	30	24	2	225

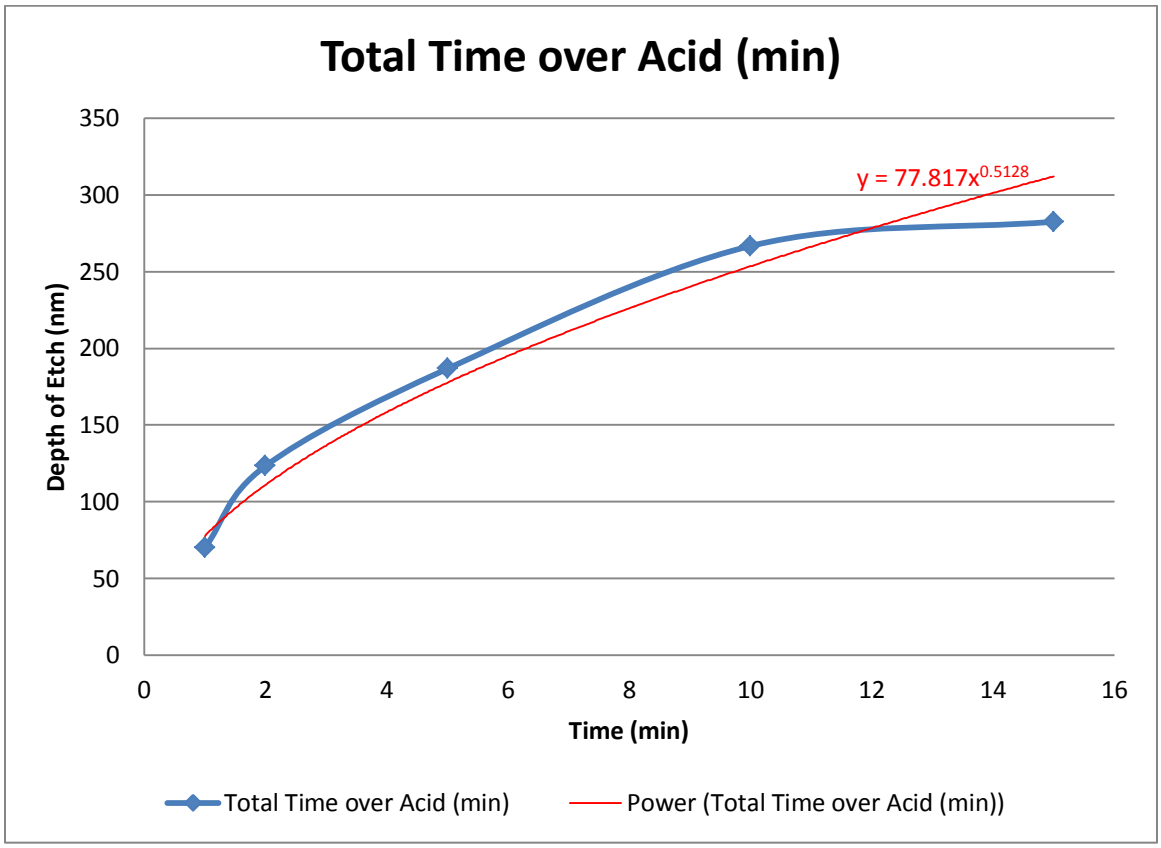

Figure 22: Depth vs. time over acid

From the data in Figure 22, the depth starts to asymptote. This is because the measurements that are being taken by the AFM are relative depths. At some point, the mask formed by the

nanoparticles becomes etched underneath from the sides - undercut. The pillars that are originally formed from the initial etching start disappearing as the undercutting becomes more severe. The longer this happens the smoother the peak gets, and the smoother the contours to the original design become.

The following figures are AFM scans from a typical slide that has been selected (Slide #99). These pictures exhibit the slide with particles prior to etching and after etching has occurred. The slides are presented in 3x3µm, 5x5µm, and 10x10µm scans. The structure of the nanoparticle mask after etching can be clearly seen. The mask was successfully created and the etching reflects the negative imprint of it.

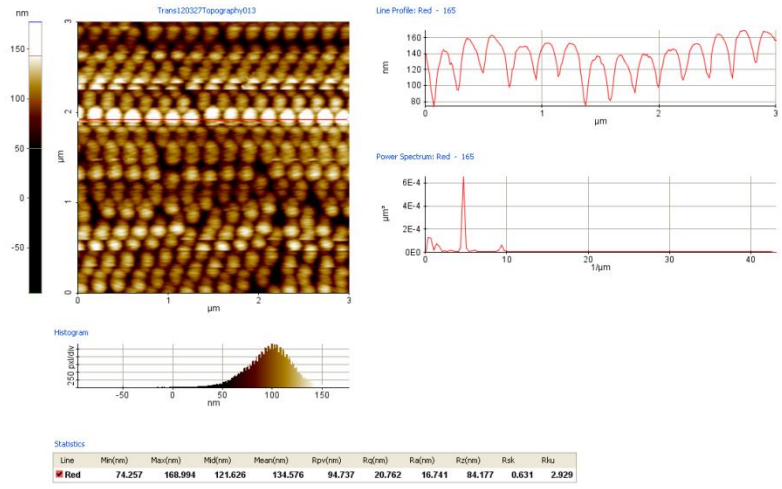

Figure 23: 3x3µm AFM Scan Pre-Etching

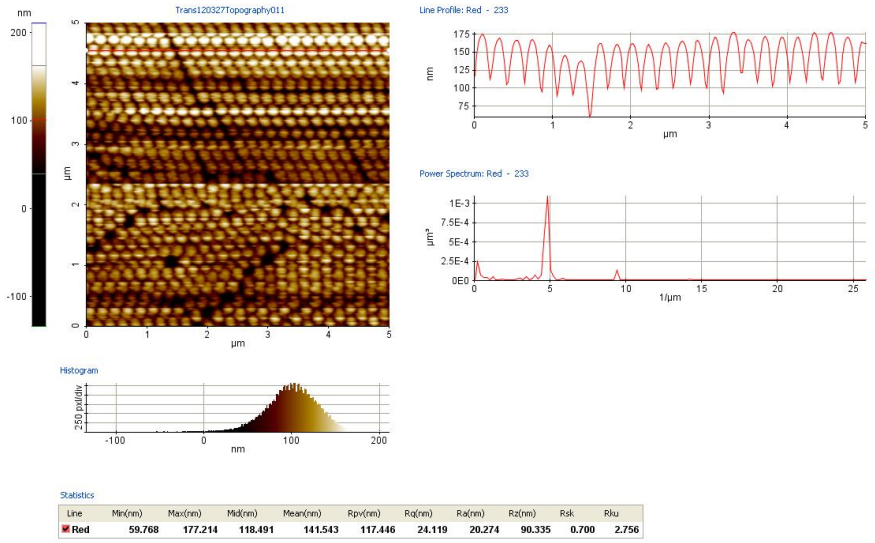

Figure 24: 5x5µm AFM Scan Pre-Etching

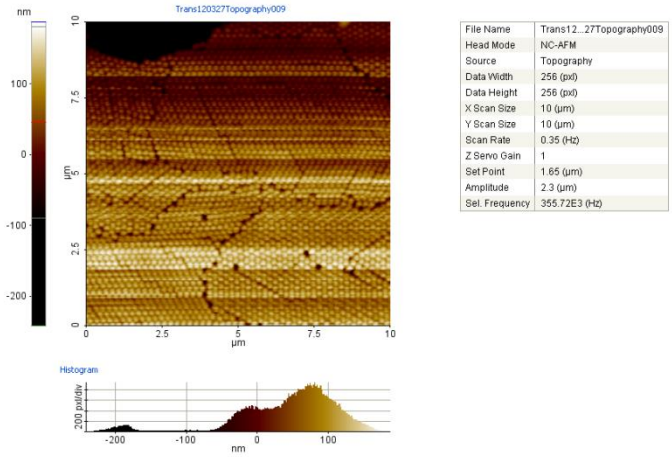

Figure 25: 10x10µm AFM Scan Pre-Etching

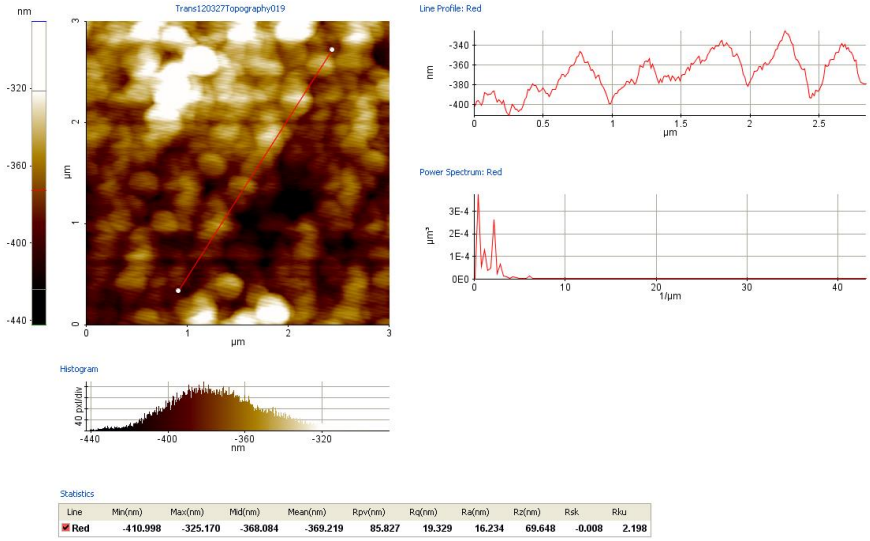

Figure 26: 3x3µm AFM scan after etching

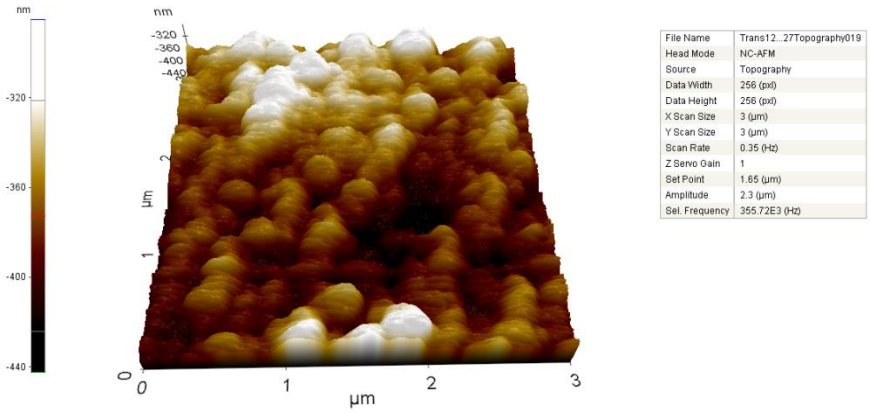

Figure 27: 3x3 AFM scan 3D view

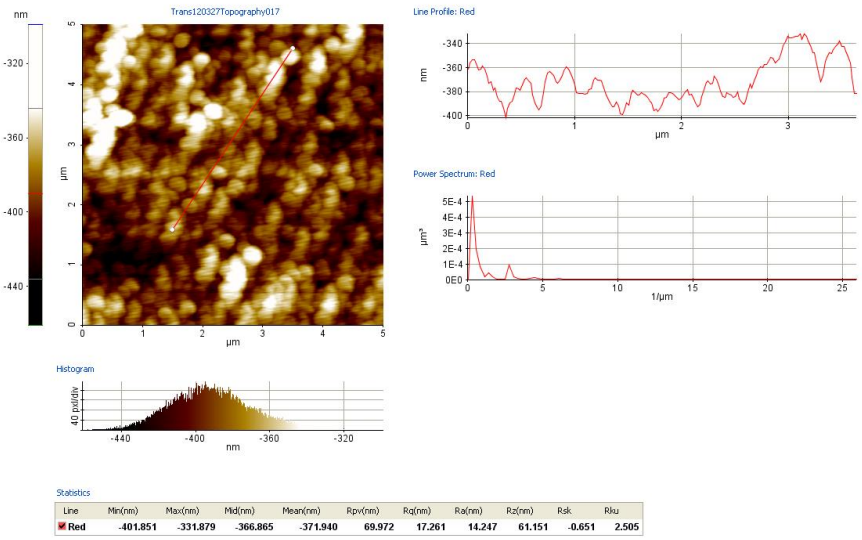

Figure 28: 5x5µm AFM line depth

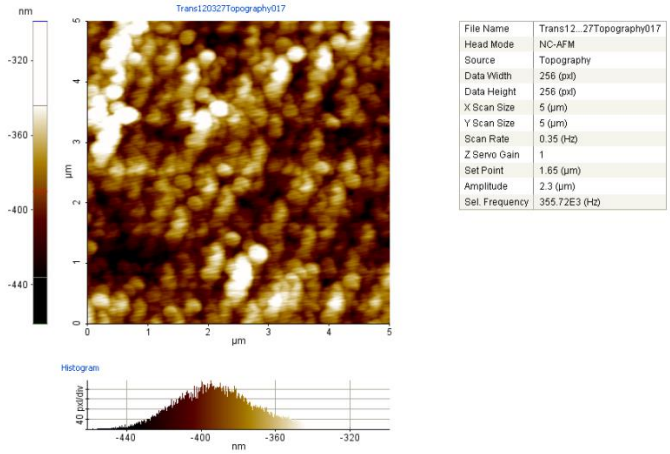

Figure 29: 5x5µm AFM Scan

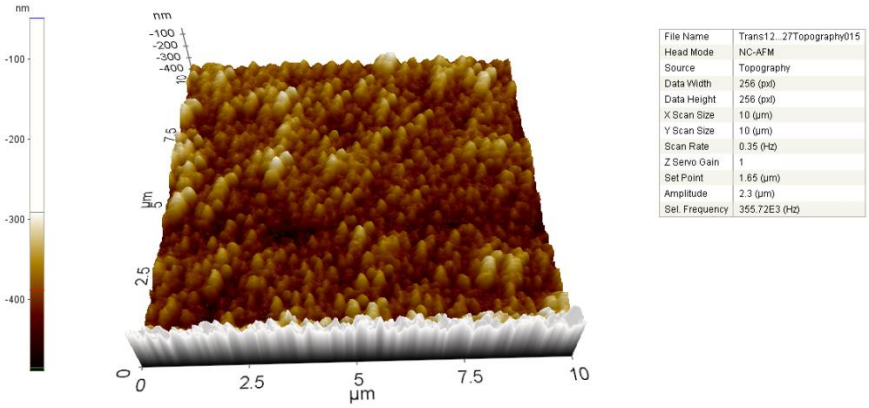

Figure 30: 3D topography 10x10µm

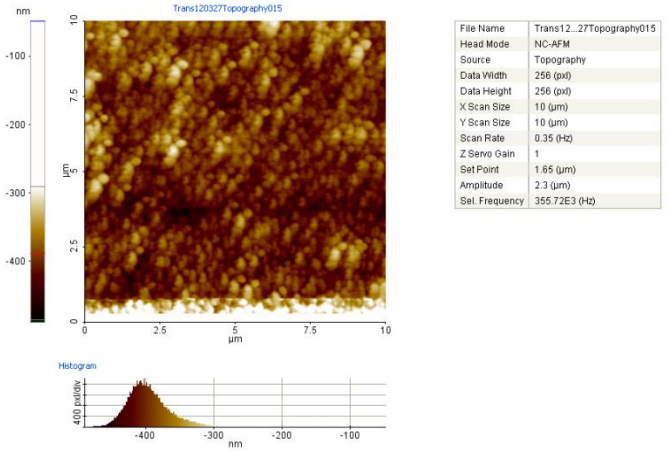

Figure 31: Topography of 10x10 µm

There are many approaches to etching silicon oxide with wet HF. There is a good study done to compare wet HF etching and vapor HF etching for silicon oxide removal in micro electro mechanical systems (MEMS). [35] The etching rates in that study are compared with the results from this research. The comparison is done using their data for thermal oxide (as deposited). This oxide is a wet thermal oxide grown at 975°C and 1200nm thick on a silicon substrate.

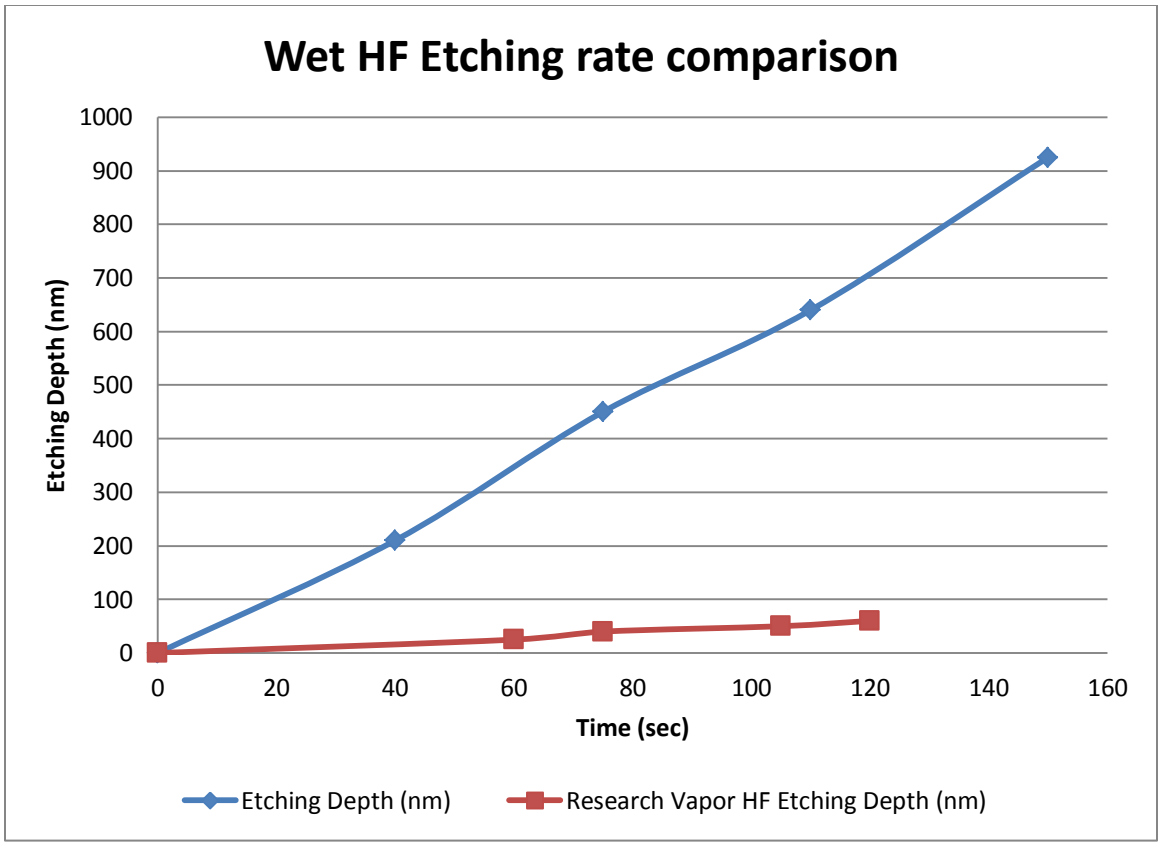

Figure 32: Etching rate of Silicon Oxide and Optical Glass

For comparison with wet etching, we used the data from Figure 22 and the results from [35]. The wet etching uses an HF:H_2O solution with a ratio 24.5%:75.5% or 14.2 mol/L. Figure 32 shows that the etch rate of vapor HF is much slower than wet HF, but more controllable. It should be noted that wet etching is not applicable in this research because it would damage the nanoparticle mask.

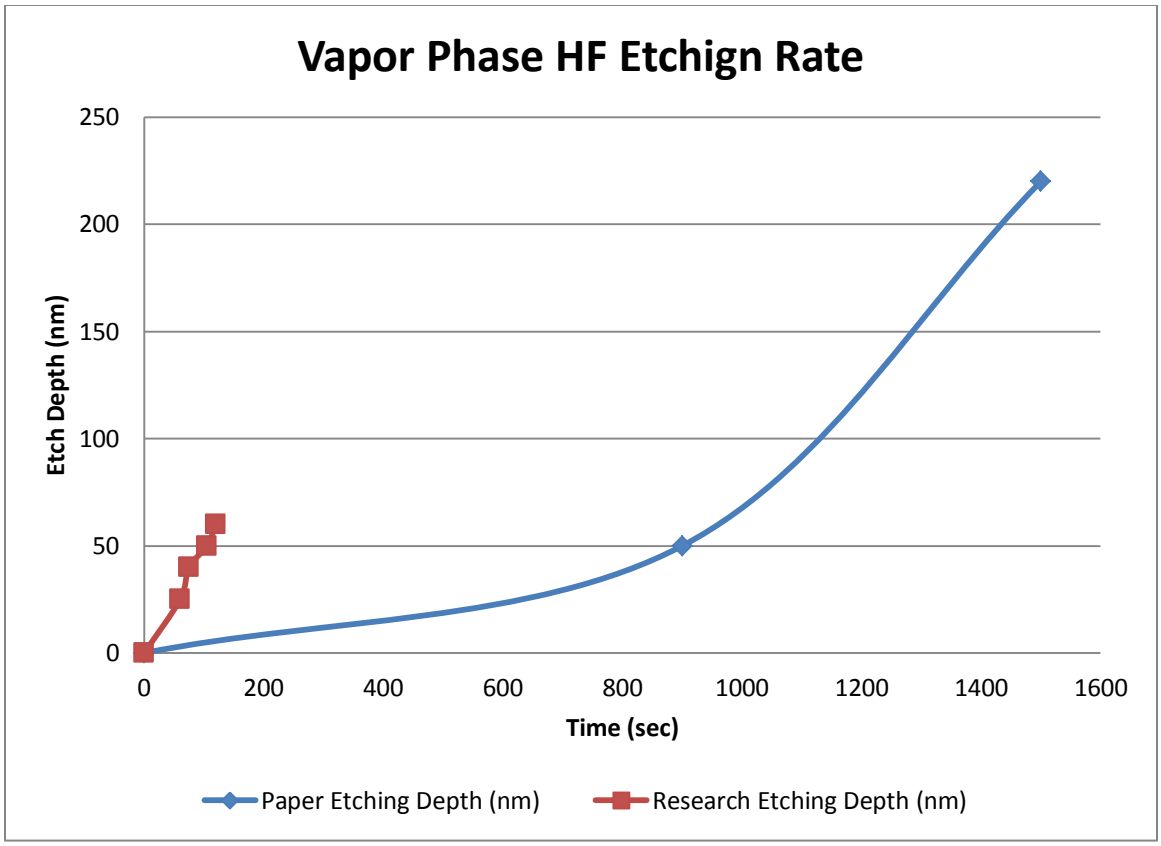

Figure 33: Vapor phase HF etching rate comparison

Comparing the data from figure 22 and the data in [35], it can be seen that the etch rate is much slower than the findings in this research. The etch rate of HF vapor is affected by the temperature of the substrate. The colder the substrate, the faster the etch rate. The etch rate from the paper was determined with a 10 min wait time over the heater stage and includes a N_2 flow for delivery of HF vapor. This dilutes the concentration per cm^3 of HF vapor per second compared to a direct delivery over HF that is vaporizing. This can be one of the main reasons why the etching performed in this research is at a more rapid rate.

Our etching rate is consistent with the results from micromachining processing (Kirt Williams, 1996) of vapor HF etching of Silicon Oxide. Their results how a 66nm/min etch rate which is almost the same as the results produced in this research.

CHAPTER 3

Testing & Measurements

3.1 Testing Procedure

In order to verify the results from etching of optical glass substrate, an optical microscope, an atomic force microscope, and a spectrometer for measuring reflectivity and transmittivity of the resulting samples were used. Using these tools, the depth of the etching, the roughness of the surface, as well as the reflectivity and transmission percentages was recorded.

3.2 Optical Microscope and Visual Analysis

After the completion of nanoparticle coating, the slide is examined through the use of an optical microscope. Although no quantitative data can be gathered from this method of testing, a preliminary qualitative examination can be done at this phase.

Using the optical microscope, the coating of nanoparticles is inspected in order to determine the uniformity of the application. Using this method, we can also observe whether or not the layer of nanoparticles is monolayer or not. If the coating is not adequate enough to be examined under the atomic force microscope, it is set aside and another slide is created in order to obtain better results.

Visual inspection is also performed by seeing changes in reflection or glare of the glass substrate with and without surface modifications. Substrates that have been modified have greatly reduced reflection and glare. Substrates that have been over etched demonstrate strong scattering properties and can be easily diagnosed with a visual inspection.

Figure 34: Pre-Etching

3.3 Atomic Force Microscope

Atomic force Microscopy is a very high resolution method of microscopy. It is capable of measuring and imaging objects on a nanoscale. The main component of the microscope is a cantilever that contains a tip that is manufactured using Microelectromechanical Systems (MEMS) technology. A laser is pointed at the tip of the cantilever and the basis for measurement is comprised of the interaction between these two parts. The cantilever taps the surface of the sample and the deflection of the tip from its home position is measured to determine the height. This is coupled with a piezoelectric scanning stage to acquire a three-dimensional image.

The atomic force microscope is the primary method that is used to determine the quantitative measurements of the experiment. The image processing tools associated with the AFM allow us to see the height profile, and roughness of the sample that we measure. This is combined with a qualitative three-dimensional rendering of the measured area for analysis. All the pictures acquired from the AFM are presented in Chapter 2.

3.4 Reflectivity and Transmission Tests

As a final test, a spectrometer is employed in order to measure how well light travels through the etched sample. A spectrometer is an instrument that implements various optical components in order to isolate specific parts of the electromagnetic spectrum. This is commonly done with mirrors and a grating that can be tilted or moved to change the specific frequency that is being isolated. After isolation, that particular wavelength of the electromagnetic spectrum can be subjected to various measurements and tests such as reflection, transmission, intensity, polarization, etc.

A Perkin Elmer Lambda900 UV/VIS/NIR spectrometer was used to test the reflectivity and transmission of the nano-optical structures within the visible spectrum of light. Transmission tests were not measured in absolute transmission, instead a baseline reading was taken from an untreated microscope slide for transmission measurements. Reflectivity measurements were not taken with an integrating sphere and so scattering losses were not accounted for. The results can be seen in the figures below:

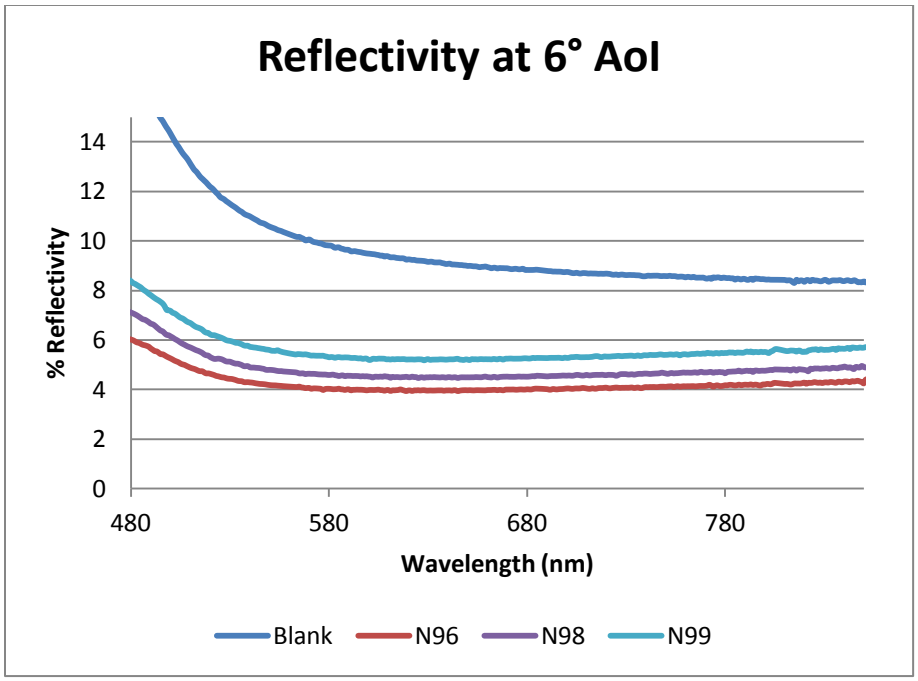

Figure 35: Reflectivity of 6° Angle of Incidence

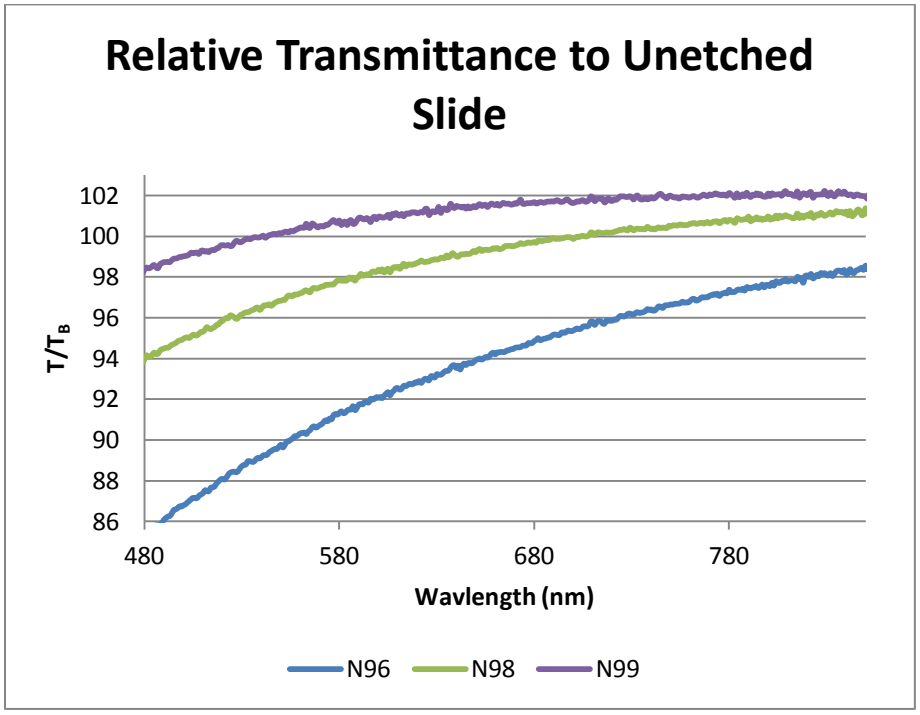

Figure 36: Relative Transmittance at 6° AoI

Figures 35 and 36 demonstrate the transmission and reflection properties of the surface modifications. Slide 99 shows enhanced transmission and reduced reflectivity over a broad

spectrum, whereas slide 98 demonstrates these qualities at longer wavelengths. All slides demonstrate anti-glare properties.

3.5 Reflectivity Simulations

The theoretical equations for single-layer optical coating have been well-developed. Reflectivity equations are well documented in standard optics books. These are referred to as Fresnel coefficients of optical interfaces. Reflectivity of the interface can be calculated from these coefficients as given by the formulas:

$$\beta = \frac{2\pi}{\lambda} n_2(\lambda) h \cos(\theta_2)$$

$$r_{12p} = \frac{n_2 \cos(\theta_1) - n_1 \cos(\theta_2)}{n_2 \cos(\theta_1) + n_1 \cos(\theta_2)}$$

$$r_{23p} = \frac{n_3 \cos(\theta_2) - n_2 \cos(\theta_3)}{n_3 \cos(\theta_2) + n_2 \cos(\theta_3)}$$

$$r_{12s} = \frac{n_1 \cos(\theta_1) - n_2 \cos(\theta_2)}{n_1 \cos(\theta_1) + n_2 \cos(\theta_2)}$$

$$r_{23s} = \frac{n_2 \cos(\theta_2) - n_3 \cos(\theta_3)}{n_2 \cos(\theta_2) + n_3 \cos(\theta_3)}$$

$$R_p = \frac{{r_{12p}}^2 + {r_{23p}}^2 + 2r_{12p}r_{23p}\cos(2\beta)}{1 + {r_{12p}}^2{r_{23p}}^2 + 2r_{12p}r_{23p}\cos(2\beta)}$$

$$R_s = \frac{{r_{12s}}^2 + {r_{23s}}^2 + 2r_{12s}r_{23s}\cos(2\beta)}{1 + {r_{12s}}^2{r_{23s}}^2 + 2r_{12s}r_{23s}\cos(2\beta)}$$

$$\bar{R} = \frac{1}{2}(R_p + R_s)$$

β is the phase difference (in radians) in the external medium between waves reflected from the first and second surfaces of the coating and h is the thickness of the modified surface layer. The first four r equations are the reflectance of each interface at a given incidence angle. The R is the average reflectance of the s and p polarizations and $\bar{R}$ is the average reflectance.

Here the novel part is the coating layer is an artificially modified surface layer. The refractive index of this layer can be calculated via:

$$n_2{}^* = [n_1{}^2(1-F) + n_2{}^2F]^{\frac{1}{2}}$$

Where n_1 is the refractive index of air, n_2 is the refractive index of the substrate, and F is the fill factor of the modified surface layer, which is the volume percentage of substrate material in the layer. [49]

As you can see, the effective refractive index can be controlled by changing the size of the nanoparticles (thereby affecting the filling factor). In addition to this index, the reflectivity can further controlled by modifying the thickness of the etched layer. Figure 37 and 38 demonstrate the effect on the reflectivity when the filling factor and thickness of the composite layer is changed. The calculations are done using MATLAB and the formulas described above. The code can be located in Appendix I.

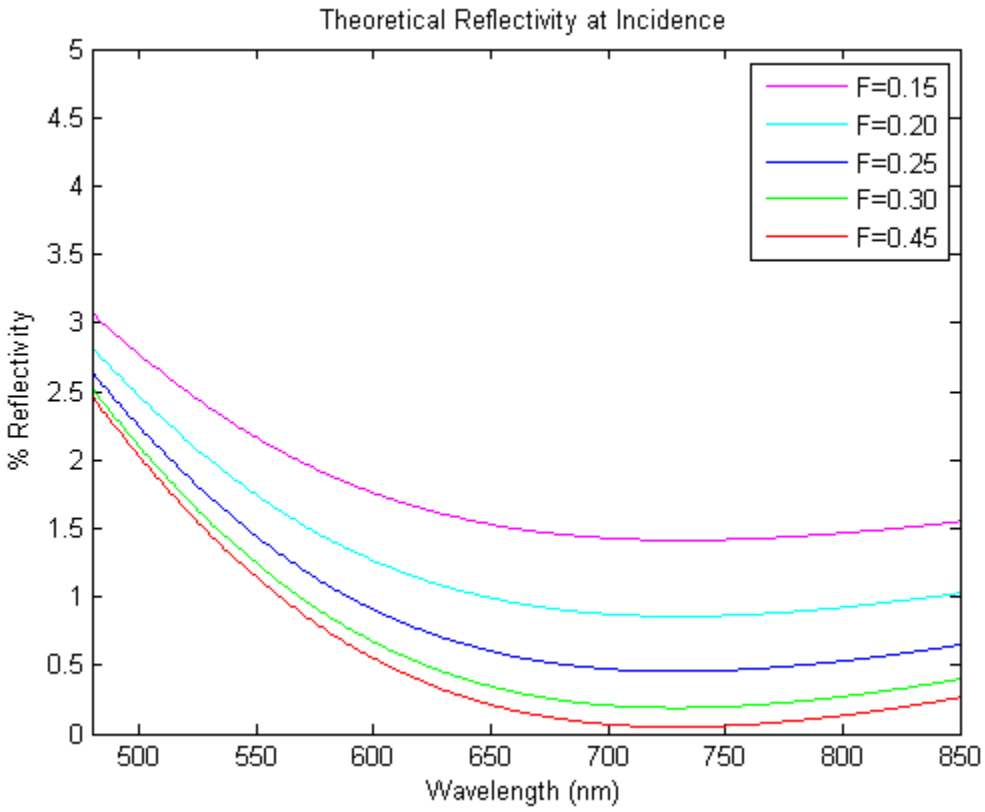

Figure 37: Theoretical Reflectivity at Incidence with given thickness of 120 nm

As you can see from figure 37, for a given thickness h = 120 nm, as the filling factor increases from 0.15 to 0.45, reflectivity decreases. Figure 38 demonstrates the effect of changing thickness on the reflectivity. For a given filling factor F=0.25, as the thickness increases the overall reflectivity increases and the shape of the curve changes (the shorter wavelengths become more reflective). Both of these figures are simulated for a single interface.

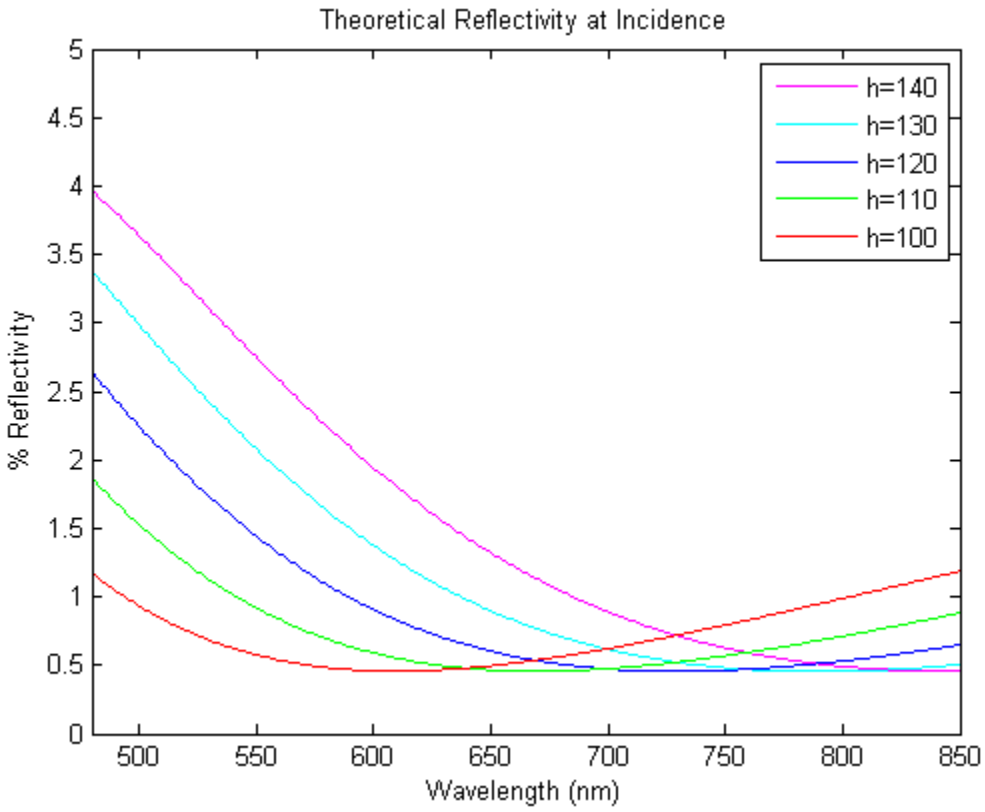

Figure 38: Reflectivity Curves with given Fill Factor F=0.25

These simulation results can be compared to the experimental measurements. Two curves are shown in Figure 39. Please note that the experimental measurement include reflections from two surfaces, one with the surface modification layer; the other is a glass and air interface. The simulations in Figure 39 have been adjusted to accommodate two surfaces. There are differences between these two curves, which are attributed to calibration error and scattering loss.

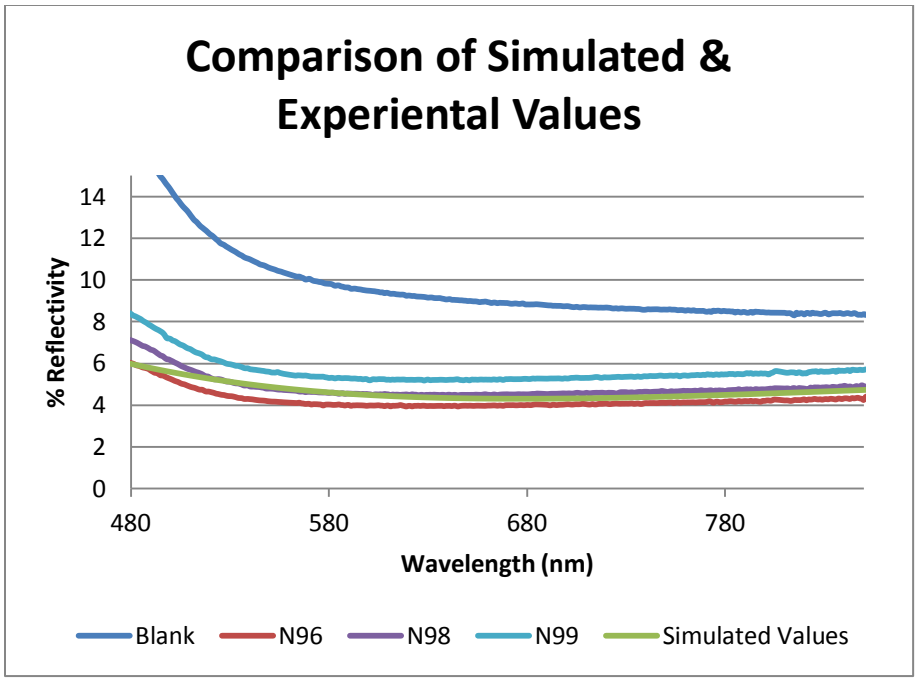

Figure 39: Comparison of simulated and experimental data

CHAPTER 4

Summary and Conclusion

4.1 Summary and Conclusion

Through the use of hydrofluoric acid vapors, fabrication of 2D nanostructures was achieved on the surface of common microscope slide glass. Nanoparticles were used as a mask for etching the structures on the slide. The mask was created via slide coating wherein capillary force was used to distribute nanoparticles as a uniform monolayer on the substrate. The resulting structure provided a pattern for HF vapors to etch the glass substrate. Nano-machining of optically transparent materially through the use of a nanoparticle mask and hydrofluoric acid vapors is a novel and successful method.

The etching rate (nm/s) of dry vapor HF etching for NSL employing less than one layer of nanoparticle mask follows a power function of $y = Ax^b$ where A is constant based on process, x is time in seconds, and b is a constant around ½. The etching rate (nm/s) of dry vapor HF etching for NSL employing one layer of nanoparticle mask is essentially linear. These formulas are valid for etching depths of less than 300 nm. The etching rate for dry vapor HF etching of microscope slides in nanosphere lithography is compared with wet HF etching of glass. Wet HF etching is shown to have an etching rate that is twenty-four times faster than the vapor HF etching of the microscope slide. The etching rate is also compared to that of dry vapor HF etching of silicon dioxide in MEMS systems. The etching rate of nanosphere lithography was shown to be faster.

The etching showed signs of a successfully transferred pattern onto the glass substrate. The modified glass substrate showed improved transmittivity and reduced reflectivity. This is a very useful property for anti-reflection and anti-glare applications. The index of refraction can be

controlled by modifying the nanosphere sizes and also the etching depths. This allows the ability to manipulate the transmission and reflection properties of the etched surface modification.

The reflectivity of the modified surfaces is calculated using MATLAB based on formulas for Fresnel coefficients and effective refractive index. Effects of the filling factor and thickness of the composite layer were studied on the reflectivity. The results were found to be in agreement with experimental measurements.

4.2 Recommendations

Creating the nanoparticle mask is a critical step for nanosphere lithography. There are a few factors affecting the quality of the mask. Temperature and humidity should be controlled in order to create a high quality slide coat over a larger area. Another factor is that the gap must be constant with the size of the nanoparticle with tolerance ±10% of the particle size between the spreader and the substrate. This affects the uniformity of the monolayer – if the gap is too big, the monolayer becomes multiple layers; if the gap is too small, the mask becomes less than one layer.

Although we present quantitative information of the etching rate, the material we used for this research is soda-lime glass and the rates will vary based on a chosen glass or pure quartz. It should also be noted that in vapor HF etching, a system with a N_2 flow to direct the HF vapors to the workpiece would allow for better control of the etching rate.

APPENDIX

I. MATLAB code to determine theoretical reflectivity

```
lambda = linspace(380,1000,621); %nm
n1 = 1.0;

F=0.25;%Fill Factor
h = 120; %nm
lambda_sq = power(lambda/1000,2); %µm
n2 = 1.5130-(0.003169*lambda_sq)+(0.003962./lambda_sq);

nf = power(((power(n1,2)*(1-F))+(power(n2,2).*F)), 0.5);

r12p = (nf-n1)./(nf+n1);
r23p = (n2-nf)./(n2+nf);
r12s = (n1-nf)./(n1+nf);
r23s = (nf-n2)./(nf+n2);

B = ((2*pi())./lambda).*n2*h;

Rp = (power(r12p,
2)+power(r23p,2)+(2.*r12p.*r23p).*cos(2*B))./(1+(power(r12p,2).*power(r23p,2)
)+(2*r12p.*r23p.*cos(2*B)));
Rs = (power(r12s,
2)+power(r23s,2)+(2.*r12s.*r23s).*cos(2*B))./(1+(power(r12s,2).*power(r23s,2)
)+(2*r12s.*r23s.*cos(2*B)));

R = 0.5*(Rp+Rs)*100;
plot(lambda, R);
xlabel('Wavelength (nm)');
ylabel('% Reflectivity');
axis([480 850 0 15]);
title('Theoretical Reflectivity at Incidence');
```

WORKS CITED

1. *"The characteristic dimensions of the nanoworld"*. **Wautelet, M and Duvivier, D.** 2007, Eur. J. Phys., Vol. 28, pp. 953-959.

2. *Comparison of the lithographic properties of positive resists upon exposure to deep- and extreme-ultraviolet radiation.* **Brainard, R.L., et al., et al.** 6, 1999, J. of Vac. Sci. & Tech. B: Microelectronics and Nanometer Structures, Vol. 17, pp. 3384-3389.

3. **Carter, J.M., et al., et al.** *"Interference Lithography"*. MIT Space Nanotechnology Laboratory, Massachusetts Institute of Technology. http://snl.mit.edu/index.html.

4. *Manufacturing with DUV lithography.* **Holmes, S.J., Mitchell, P.H. and Hakey, M.C.** 1.2, 1997, IBM J. Res. Develop., Vol. 41, pp. 7-19.

5. *Real-time spatial-phase locking for vector-scan electron beam lithography.* **Yang, Yugu and Hastings, J.T.** 6, Nov/Dec 2007, Journal of Vacuum Science and Technology B, Vol. 25, pp. 2072-2076.

6. *Resolution limits for electron-beam lithography.* **Broers, A. N.** 1988, IBM Journal of Research and Development, Vol. 32, pp. 502-504.

7. *"Electron beam lithographyresolution limits"*. **Broers, A.N., Hoole, A.C.F. and Ryan, J.M.** 1996, Microelectronic Engineering, Vol. 32, pp. 131-141.

8. *High-throughput NGL electron-beam direct-write lithography system.* **Parker, N.W. and et al.** 2000. Proc. SPIE 3997. p. 731.

9. **McCord, M.A. and Rooks, M.J.** *SPIE Handbook of Microlithography, Micromachining, and Microfabrication.* [ed.] P. Rai-Choudhury. 2000. pp. 128-252. Vol. 1.

10. *Nanosphere Lithography: Size-Tunable Silver Nanoparticle and Surface Cluster Arrays.* **Hulteen, J.C., et al., et al.** 1999, J. Phys. Chem. B, Vol. 103, pp. 3854-3863.

11. *Nanosphere lithography: fabrication of large-area Ag nanoparticle arrays by convective self-assembly and their characterization by scanning UV-visible extinction spectroscopy.* **Ormonde, A.D., et al., et al.** 16, Aug 3, 2004, Langmuir, Vol. 20, pp. 6927-6931.

12. *Fabrication of Size-Tunable Gold Nanoparticles Array with Nanosphere Lithography, Reactive Ion Etching, and Thermal Annealing.* **Tan, B.J.Y., et al., et al.** 22, 2005, J. Phys. Chem. B, Vol. 109, pp. 11100-11109.

13. *Fabrication of Large-Area Ferromagnetic Arrays Using Etched Nanosphere Lithography.* **Weekes, Shemaiah M., Ogrin, Feodor Y. and Murray, William A.** 25, 2004, Langmuir, Vol. 20, pp. 11208-11212.

14. *Problems of the nanoimprinting technique for nanometer scale pattern definition.* **Scheer, H.C. and Schulz, H.** 1998, Journal of Vacuum Science and Technology B, pp. 3917-3921.

15. *"Recent progress in nanoimprinting technology and its applications".* **Guo, L. J.** 2004, J. Phys. D: Appl. Phys., Vol. 37, pp. 123-141.

16. *"Imprint of sub-25 nm vias and trenches in polymers".* **Chou, S.Y., Krauss, P.R. and Renstorm, P.J.** 1995, Appl. Phys. Lett., Vol. 67, p. 3114.

17. **Chou, S.Y., Krauss, P.R. and Renstorm, P.J.** "Imprint Lithography with 25-Nanometer Resolution". *Science.* 1996, Vol. 272, p. 85.

18. **Cheng, X and Guo, L J.** "One-Step Lithography for Various Size Patterns with a Hybrid Mask-Mold". *Microelectron. Eng.* 2004, Vols. 71(3-4), pp. 288-293.

19. *"Combined nanoimprint-and-photolithography technique with a hybrid mold".* **Cheng, X, Chang, M-H and Guo, L J.** 2004. Proc. SPIE. Vol. 5374, pp. 337-347.

20. *Macroscopic Arrays of Magnetic Nanostructures from Self-Assembled Nanosphere Templates.* **Weekes, Shemaiah M., et al., et al.** 23, 2007, Langmuir, pp. 1057-1060.

21. *Fabrication of High-Quality Opal Films with Controllable Thickness.* **Gu, Zhong-Ze, Fujishima, Akira and Sato, Osamu.** 2, 2002, Chem. Mater., Vol. 14, pp. 760-765.

22. *Thoery of Stability of Lyophobic Colloids.* **Verwey, E.J.W.** 3, March 1947, J. Phys. Chem., Vol. 51, pp. 631-636.

23. *Theory of the stability of strongly charged lyophobic sols and of the adhesion of strongly charged particles in solutions of electrolytes.* **Derjaguin, B. and Landau, L.** 1-4, 1993, Progress in Surface Science, Vol. 43, pp. 30-59.

24. *Order and Disorder in Liquid Solutions.* **Kirkwood, John G.** 1, 1939, J. Phys. Chem., Vol. 43, pp. 97-107.

25. *Phase Transition in Elastic Disks.* **Alder, B. J. and Wainwright, T. E.** 1962, Phys. Rev., Vol. 127, pp. 359-361.

26. *Two-dimensional colloidal crystal corrugated waveguides.* **Zhao, Yang and Avrutsky, Ivan.** 12, June 15, 1999, Opt. Lett., Vol. 24, pp. 817-819.

27. *Optical coupling between monocrystalline colloidal crystals and a planar waveguide.* **Zhao, Y., Avrutsky, I. and Li, B.** 1999, Appl. Phys. Lett, Vol. 75, p. 3596.

28. *Optical demultiplexing in a planar waveguide with colloidal crystal.* **Avrutsky, Ivan, Kochergin, Vladimir and Zhao, Yang.** 12, December 2000, Photon. Tech. Lett., IEEE, Vol. 12, pp. 1647-1649.

29. **Nakamura, Hiroshi.** *Colloidal Crystals-Self-Assembly of Monodispersed Colloidal Particles.* s.l. : R&D Review of Toyota CRDL, 2004. Vol. 39, No. 4.

30. **Yates, M. Z., et al., et al.** *Self-assembly of coated colloidal particles for optical applications.* s.l. : LLE Review, 2003. pp. 28-35. Volume 97.

31. *Block copolymer lithography: Periodic arrays of [approximately]1011 holes in 1 square centimeter.* **Park, M, et al., et al.** s.l. : Science, 1997, Vol. 276, pp. 1401-1404.

32. *Mechanism of formation of two-dimensional crystals from latex particles on substrates.* **Denkov, N., et al., et al.** 12, 1992, Langmuir, Vol. 8, pp. 3183-3190.

33. *Formation of two-dimensional structures from colloidal particles on fluorinated oil substrate.* **Lazarov, Genady S., et al., et al.** 14, 1994, J. Chem. Soc., Faraday Transactions, Vol. 90, pp. 2077-2083.

34. *Porous silica via colloidal crystallization.* **Velev, O. D., et al., et al.** October 2, 1997, Nature, Vol. 389, pp. 447-448.

35. *A comparison between wet HF etching and vapor HF etching for sacrificial oxide removal.* **Witvrouw, A., et al., et al.** Santa Clara : Micromachining and Microfabrication Process Technology VI, 2000. Proc. SPIE. Vol. 4174, p. 130. doi:10.1117/12.396423.

36. **Klein, M. and Furtak, T.** *Optics.* 2nd. s.l. : John Wiley & Sons, Inc., 1986. ISBN: 978-0-471-87297-9.

37. *Reflection properties of nanostructure-arrayed silicon surfaces.* **Hadobás, K., et al., et al.** 3, September 2000, Nanotechnology, Vol. 11, pp. 161-164.

38. **Lalanne, Philippe and Hutley, Mike.** *"Artificial Media Optical Properties—Subwavelength Scale" in Encyclopedia of Optical Engineering.* s.l. : Dekker, 2003. pp. 62-71.

39. *Homogeneous layer models for high-spatial-frequency dielectric surface-relief gratings: conical diffraction and antireflection designs.* **Brundrett, David L., Glytsis, Elias N. and Gaylord, Thomas K.** 13, 1994, Applied Optics, Vol. 33, pp. 2695-2706.

40. *Diffractive Optics and Micro-Optics: Introduction to the Feature Issue.* **Magnusson, Robert and Gale, Michael T.** 32, 2001, Applied Optics, Vol. 40, pp. 5817-5818.

41. *Optimal design for antireflective tapered two-dimensional subwavelength grating structures.* **Grann, Eric B., Varga, M. G. and Pommet, Drew A.** 2, 1995, JOSA A, Vol. 12, pp. 333-339.

42. *Homogeneous layer models for high-spatial-frequency dielectric surface-relief gratings: conical diffraction and antireflection designs.* **Brundrett, David L, Glytsis, Elias N and Gaylord, Thomas K.** 13, 1994, Applied Optics, Vol. 33, pp. 2695-2706.

43. *Engineering photonic nanostructure profiles using nanosphere lithography and reactive-ion etching.* **Wang, Jinsong, Zhao, Yang and Mao, Guangzhao.** Bellingham : s.n., 2006. Proceedings of SPIE Vol. 6308.

44. *Binary gratings with increased efficiency.* **Farn, Michael W.** 22, 1992, Applied Optics, Vol. 31, pp. 4453-4458.

45. *Binary subwavelength diffractive-lens design.* **Mait, Joseph N., Prather, Dennis W. and Mirotznik, Mark S.** 17, 1998, Optics Letters, Vol. 23, pp. 1343-1345.

46. *Antireflection behavior of silicon subwavelength periodic structures for visible light.* **Lalanne, Philippe and Morris, G. Michael.** 2, 1997, Nanotechnology, Vol. 8, p. 53.

47. *Fabrication and Simulation of Diffractive Optical Elements with Superimposed Antireflection Subwavelength Gratings.* **Nikolajeff, Fredrik, et al., et al.** 26, 2000, Applied Optics, Vol. 39, pp. 4842-4846.

48. *Broadband antireflection gratings fabricated upon silicon substrates.* **Kanamori, Y, Sasaki, M and Hane, K.** 1999, Opt. Lett., Vol. 24, pp. 1422-1424.

49. *Colloidal subwavelength nanostructures for antireflection optical coatings.* **Zhao, Y, Wang, J and Mao, G.** 2005, Opt. Lett., Vol. 30, pp. 1885-1887.

50. *Nanostructure fabrication using nanosphere lithography for photonic devices.* **Wang, J, Mao, G and Zhao, Y.** Long Beach : CLEO/QELS 06, 2006.

51. *Engineering photonic nanostructure profiles using nanosphere lithography and reactive-ion etching.* **Wang, J and Zhao, Y.** San Diego : SPIE, 2006. Vol. 6308.

52. *Antireflection behavior of silicon subwavelength periodic structures for visible light.* **Lalanne, Philippe and Morris, G Michael.** 2, 1997, Nanotechnology, Vol. 8, pp. 53-56. ISSN.

53. *Nanowire photonics.* **Pauzauskie, P.J. and Yang, P.** 10, 2006, Materials Today, Vol. 9, pp. 36-45.

54. *Controlling the Interaction between Light and Gold Nanoparticles: Selective Suppression of Extinction.* **Linden, S., Kuhl, J. and Giessen, H.** 20, May 14, 2001, Phys. Rev. Lett., Vol. 86, pp. 4688-4691.

55. *Fabrication of Photonic Crystal Lasers by Nanomolding of SolGel Glasses.* **Schueller, Olivier J.A., et al., et al.** 27, 1999, Applied Optics, Vol. 38, pp. 5799-5802.

56. *Effects of intrinsic hydrophobicity on wettability of polymer replicas of a superhydrophobic lotus leaf.* **Kwon, Tai Hun and Lee, Seung-Mo .** 4, 2007, Journal of Micromechanics and Microengineering, Vol. 17, p. 687.

57. *"Fabrication of Centimeter-Sized Single-Domain Two-Dimensional Colloidal Crystals in a Wedge-Shaped Cell under Capillary Forces".* **Sun, Jie, et al., et al.** 11, s.l. : American Chemical Society, 2010, Langmuir, Vol. 26, pp. 7859-7864. DOI: 10.1021/la9047165.

ABSTRACT

FABRICATION OF TWO-DIMENSIONAL NANOSTRUCTURES ON GLASS USING NANOSPHERE LITHOGRAPHY

by

ELMER WANG

August 2013

Advisor: Dr. Yang Zhao

Major: Electrical Engineering

Degree: Master of Science

It is desired to have artificial optical materials with controllable optical properties. One approach is to create composite materials with nanomachining and nanostructures. In this research, two-dimensional (2D) nanostructures were created on the surface of optical glass using nanosphere lithography. In comparison with conventional techniques, this approach is more efficient and cost-effective for the creation of large areas of thin surface layers as an artificial material. A uniform monolayer of 200 nm polystyrene nanospheres was deposited on soda-lime glass slides. Deposition was performed via a slide-coating technique to take advantage of capillary forces. The slides were etched with vapor-phase hydrofluoric acid (HF) to create 2D structures. Vapor-phase etching was selected in order to etch the substrate without disturbing the monolayer nanoparticle mask. The etching rate of nanostructures was studied. An atomic force microscope (AFM) was used to monitor the nanosphere monolayers and etching analysis. It was shown that the nanoparticle pattern was successfully transferred to the surface of the substrate. The resultant thin-layer of modified substrate serves as an artificial material with a desired refractive index which modifies the surface reflection and transmission properties. The effective

refractive index of the artificial layer is smaller than the refractive index of the substrate and can be varied by changing the size of the nanoparticles and depth of etching. The substrate with the created artificial material layer demonstrated reduced reflectivity in optical wavelengths.